

Quantum transport theory of electrons in solids: A single-particle approach

Jørgen Rammer

Department of Physics and Materials Research Laboratory, University of Illinois at Urbana-Champaign, Urbana, Illinois 61801

and Institutt for Fysikk, Universitetet i Trondheim, Norges Tekniske Høgskole, N-7034 Trondheim, Norway*

The electronic transport theory of semiconductors is not, from a first-principles point of view, as well understood as is that of metals, where the degeneracy of the Fermi system leads to a simplified but comprehensive theory. In the case of semiconductors, degeneracy usually plays no simplifying role at all. However, in many transport problems of current interest one is effectively dealing with the equivalent of a single particle interacting with an environment, e.g., a heat bath or a random potential. In view of this, the author presents a simple formalism for the quantum dynamics of a single continuous degree of freedom. The quantum-statistical description is in terms of the density matrix, and the Feynman rules for a standard treatment of the density matrix are presented and illustrated by applications to problems of current interest. It is shown that such an effect as, for example, the intracollisional field effect, which in the past has been dealt with using complicated formalisms, in the present treatment is described in an elementary way. The single-particle approach conveniently displays the interference aspect of quantum-mechanical transport, as is discussed in a treatment of the weak localization effect in disordered conductors. The real-space representation of quantum transport is stressed, as is appropriate for a proper discussion of mesoscopic physics. The author treats the connection between the linear-response formalism and the Landauer approach by expressing the conductance in terms of the scattering properties of a sample. He also discusses the conductance fluctuations of mesoscopic samples.

CONTENTS

I. Introduction	781
II. Density-Matrix Description of Quantum Dynamics	782
A. Reduced density-matrix description of a particle interacting with a heat bath	782
B. Feynman diagrammatics for the reduced density matrix	783
C. Temporal evolution on differential form of the reduced density matrix and the corresponding diagrammatic representation	788
III. The Kinetic Approach	790
A. The Wigner function	790
B. The intracollisional field effect for electron-phonon interaction	791
IV. Density-Matrix Description of a Particle in a Random Potential	793
A. Feynman rules for the impurity-averaged density matrix	793
B. Quantum kinetic equation for weak impurity scattering	795
V. Linear Response of Disordered Conductors	797
A. The conductivity tensor	797
B. The classical conductance	800
C. Weak localization	801
D. Landauer conductance formula	806
E. Conductance fluctuations	809
VI. Summary and Conclusion	814
Acknowledgments	815
References	815

I. INTRODUCTION

In recent years, great progress in controlled construction of new and smaller material structures has been

made possible by the introduction of fabrication techniques such as, for example, molecular-beam epitaxy. To describe electronic transport in these new artificial submicron structures, in many cases we cannot resort to a classical Boltzmann description but must include the quantum-mechanical aspects of electronic transport. For reasons of material and device functioning, semiconductor materials play a major role in this new development. The important quantum aspects of electronic transport in these structures are therefore those associated not with the degeneracy of the Fermi system, but rather with the interference aspect of quantum mechanics.

A wide variety of electronic quantum transport problems of current interest in solid-state physics are essentially one particle in nature. A full many-body formalism to treat such problems, formulated conveniently in terms of the many-body Green's functions (Abrikosov *et al.*, 1965), is therefore not mandatory, since such complete information is unnecessary. This observation would only be a matter of simplification if we always had controlled approximation schemes for converting a first-principles, full many-body formulation into a manageable form for extracting information about the transport properties in a general nonequilibrium state. This, however, is not the case for the important area of electronic transport in semiconductors.

For the case of metals, both for the normal and the superconducting state (Eliashberg, 1971), we have a consistent approximation scheme that allows us to reduce the full many-body problem to a manageable form under the minor restriction that we consider only states that are perturbed on length scales larger than atomic distances. But the very nature of semiconducting materials excludes them from such a scheme. The physical reason for the

*Present address.

existence of a successful approximation scheme for the case of metals is the fact that we are here dealing with a degenerate Fermi system in which all relevant energy scales are small compared to the Fermi energy. In consequence, the kinematics is essentially quasiclassical, and a consistent and compact description of the transport properties of metals over essentially all ranges of parameters can be obtained, elegantly formulated in terms of the so-called quasiclassical Green's functions. The only severe limitation of the quasiclassical theory is its inherent assumption of particle-hole symmetry, so that within the quasiclassical scheme all thermoelectric coefficients vanish, and no conclusions can be drawn about many-body effects on the thermoelectric properties. Similarly, the degeneracy assumption does not allow for immediate inclusion of the orbit-bending property of a magnetic field. A remedy to these limitations has been suggested for special cases (Eckern and Schmid, 1981). A recent review of the quasiclassical method applied to metals is that of Rammer and Smith (1986).

The full many-body Green's-function approach is clearly just as valid a starting point for the study of transport in semiconductors as for the case of metals. However, the approach is not as fruitful, since irrelevant information cannot in general be eliminated in a controlled manner to obtain a manageable description of nonequilibrium states of interest as in the case of metals or other degenerate Fermi systems, such as, for example, normal and superfluid ^3He (Serene and Rainer, 1983). Furthermore, in many cases of interest, the nondegenerate limit is considered, and the inclusion of the Pauli principle in the description is irrelevant.

In view of these features of electronic transport in semiconductors, a description of electronic transport in solids that makes use of the one-particle simplification from the very outset would seem desirable. We present such a description below. That is, as far as the electronic system is concerned, we are dealing with one-particle properties. Clearly, a first-principles treatment of the electron-electron interaction requires the full many-body formulation. However, even when the electron-electron interaction is of importance, a one-particle formulation is often adequate for the calculation of specific properties. The electron-electron interaction can, for particular situations, be dealt with separately, say in the random-phase approximation, resulting in an effective bosonic interaction. For the calculation of specific physical properties the effect of the electron-electron interaction can then be ascertained at the one-particle level. An example of a case in which such a mean-field description is sufficient is the calculation of the phase-breaking rate due to the electron-electron interaction in weak localization theory (Al'tshuler, Aronov, and Khmel'nitskii, 1982). The rationale for the approach is that, in describing transport in a nondegenerate Fermi system, there is no generally valid consistent approximation scheme. Therefore a simple and physically transparent description, though limited in scope, is valuable for the simplifications it affords in each

particular transport situation. In the following, we shall be dealing with the nonequilibrium quantum-statistical mechanics of a single degree of freedom, and we shall demonstrate that this allows a treatment that employs only elementary methods of quantum mechanics and statistics. However, we shall employ a field-theoretic language, thereby demonstrating its usefulness in a quantum-mechanical context. An acquaintance with the following formalism apart from its own merit, should therefore be helpful to the reader with interests in the application of quantum field-theoretical methods in transport theory, since the complicating temporal aspect of quantum dynamics is the same in both quantum mechanics and quantum field theory.

At this point, we note that we shall favor a real-time formulation of the nonequilibrium problem, since it constitutes a direct physical representation. We thus prefer that the doubling of the degrees of freedom characteristic of a treatment of nonequilibrium states be generated by the quantum dynamics itself. The presentation parallels previous discussions of nonequilibrium statistical physics, since in essence it is an application of the methods of Schwinger (1961), Feynman (1963, 1965), and Keldysh (1964) to the physical problem of concern.

The quantum-statistical mechanics of a single degree of freedom is described by the density matrix. Density-matrix description dates back to the early development of quantum mechanics (Landau, 1927; von Neumann, 1932). Up until recently most electronic transport properties of solids could quite adequately be accounted for classically and dealt with through the Boltzmann description, and the density-matrix approach was used to justify such quasiclassical descriptions as appropriate limits of the quantum-mechanical description (Greenwood, 1958). The Boltzmann description can be successfully applied even to strong-coupling situations after suitable renormalization as for instance in the case of strong electron-phonon interaction (Prange and Kadanoff, 1964), and the polaron problem (Kadanoff and Revsen, 1964; Langreth, 1967). It is even successful when the underlying equilibrium state is quite exotic and owes its very existence to quantum-mechanical effects. This is, for example, the case for the superconducting and superfluid states, where a Boltzmann description in terms of the quasiparticle excitations of the equilibrium state accounts quite well for a vast range of nonequilibrium phenomena in superconductors and superfluids. However, over the last decade we have witnessed a wealth of transport phenomena that are genuine manifestations of quantum-mechanical interference, and we shall see below how the density-matrix method can also provide a useful description of quantum transport. In particular, we shall take advantage of a diagrammatic technique that enhances physical insight into the phenomena over that possible with purely algebraic formulations of quantum mechanics. The diagram technique we shall introduce is considerably simpler than the one introduced by Konstantinov and Perel (1960), as we use the closed-time-path

formulation of Schwinger (1961) and consequently introduce only real times. The diagrammatic approach to the density matrix was used by Iche and Nozières (1978) to study the quantum Brownian motion of a heavy particle. In the following we shall present the general diagrammatic description, apply it to the electron-phonon interaction in external fields, and give a detailed description of the physics of disordered conductors.

Due to technological advances in the fabrication of submicron structures, the study of quantum transport in strong electric fields has grown in importance; we shall show how the intracollisional field effect is easily dealt with by the presented formalism, with no more labor than that involved in obtaining the usual Boltzmann limit. The intracollisional field effect was considered for the many-electron case by Barker (1973). He derived the kinetic equation by the use of the super-operator method, which provides a proper description. However, this method lacks physical transparency, and, as already noted, we prefer to have the quantum dynamics directly double the degrees of freedom necessary for the description of nonequilibrium states, as this allows for a direct physical interpretation. The intracollisional field effect was considered first at the one-electron level by Levinson (1969).

Another reason for illustrating the method to be presented by applying it to the intracollisional-field-effect problem is that recent applications of the nonequilibrium many-body Green's-function technique have given erroneous results, as noted by Jauho and Wilkins (1984). The reason for this is precisely the uncontrolled approximations alluded to above. The very introduction of a distribution function that depends on only one time variable (usually euphemized as an "ansatz") is a crucial step in obtaining a quantum kinetic equation from the full many-body Green's-function description. Lipavsky *et al.* (1986) demonstrated how to make the choice such that the ensuing kinetic equation agrees with the result of the super-operator method for the case of the intracollisional field effect. A similar but more general choice was used by Al'tshuler (1978), based on the kind of decomposition used in the quasiclassical theory of electronic transport in metals. In the quasiclassical theory the systematics of such a decomposition can be explicitly demonstrated, as shown by Shelankov (1985), whereas in the general case one is restricted to almost homogeneous nonequilibrium states, the gradient approximation. The question arises whether a systematic decomposition in terms of a single-time distribution function is possible quite generally in the many-body case. The answer to this question is no. In the general case the distribution function will depend on two time variables. An affirmative answer would be tantamount to a fluctuation-dissipation theorem for general nonequilibrium states. The problem is that we need correlation functions to describe the full many-body transport situation in quantum mechanics, and for general nonequilibrium states we have no general scheme for decomposing the correlation

function into parts describing instantaneous quantum states and their occupation. In the one-electron theory to be presented, this decomposition problem never arises, as we are dealing directly with the density matrix. The theory to be presented is therefore particularly important in cases where the treatment of the many-electron problem is nontrivial.

We shall use the diagrammatic technique to discuss the physics of disordered conductors. Besides providing a simple framework for performing quantitative calculations in this important area of quantum transport, the diagrammatic approach leads to very useful physical pictures of quantum transport in random media. In particular, it gives a simple geometric interpretation for the theory of weak localization.

Due to the smallness of a structure, the electronic transport through it can take place quantum mechanically coherently. This is the regime of mesoscopic physics, where the individual features of a structure, such as geometry, distinct impurity configuration, etc., are manifested in the transport properties of the structure. The properties of mesoscopic systems can in many cases be adequately discussed in terms of single-electron properties. In certain cases, the influence of the environment, for example its temperature, can be assessed by simple means; however, in general, the full quantum-statistical mechanics of a single degree of freedom will be necessary. It is therefore of importance to pursue a description that favors transparency in order to allow for immediate physical interpretation, especially with respect to the interference aspect of quantum transport. In the following we describe how the standard method of nonequilibrium statistical mechanics can be formulated to deal effectively with such situations; in particular, we shall obtain a representation of the density matrix in terms of standard Feynman diagrams. The finite size of mesoscopic systems makes the choice of appropriate boundary conditions particularly by important. Therefore, in our presentation we shall emphasize the real-space representation, in which boundary conditions can be properly imposed as illustrated by deriving from the linear-response theory the scattering formula for the conductance, central to the Landauer approach to quantum transport. Likewise, the real-space representation is necessary for the description of mesoscopic fluctuations, and we describe in detail the quantum-interference-induced conductance fluctuations.

We believe that the formalism to be presented is relevant to quantum transport theory in general. It does not deal with degeneracy, which in many cases is irrelevant, but offers a gain in simplicity and clarity in displaying the interference features of quantum-mechanical transport.

In the following we describe the single-particle approach to quantum transport and by using only elementary methods develop a formalism that allows a comprehensive quantitative discussion of problems of current interest in transport theory. Several of these to-

pics are presented in the literature in their quantum field-theoretic context. Here we shall present the same topics in a quantum-mechanical context and, in a simple fashion, create the apparatus for performing quantitative calculations. In Sec. II we introduce the density-matrix description of the dynamics of a particle coupled to a heat bath and derive its Feynman diagrammatics. In Sec. III we describe the kinetic-equation approach to quantum transport, and to illustrate the method we treat the problem of a particle in an external field weakly coupled to a heat bath. Section IV treats the density-matrix description of a particle in a random potential. The intracollisional field effect is immediately included in the approach. In Sec. V, we use the diagrammatic approach to discuss linear-response theory. In particular, we present the general one-particle theory of conductivity necessary for a discussion of the conduction properties of disordered conductors. The quantum interference phenomena of weak localization are discussed with particular emphasis on the quantum-interference-induced anomalous magnetoresistance. The mesoscopic phenomena of disordered conductors are discussed, and contact between the conventional Hamiltonian linear-response theory and the Landauer approach to quantum transport is made. We end the section on disordered conductors by discussing quantum-interference-induced conductance fluctuations. Section VI offers a summary and conclusions.

II. DENSITY-MATRIX DESCRIPTION OF QUANTUM DYNAMICS

In this section we present, in a form suitable for our purpose, the basic notions of the quantum-mechanical description of physical states for which only partial information is available, or for which only some of the information is relevant to the situation in question. In such a case, a description in terms of wave functions or, equivalently, projection operators, must be abandoned in favor of a quantum-statistical description in terms of the statistical operator. Knowledge of the statistical operator allows us to assess only the probabilities for the occurrence of a given state and not, as in quantum mechanics, the relative phases between state vectors constituting a superposition. We have in mind situations in which measurements are performed only on the electronic degrees of freedom of the solid, such as, for instance, in an electrical conductivity measurement, and the physical quantity of interest can therefore be expressed in terms of the reduced statistical operator for the electron, not explicitly involving the lattice degrees of freedom.

A. Reduced density-matrix description of a particle interacting with a heat bath

Let us consider a single continuous quantum-mechanical degree of freedom, labeled by coordinate x and referred to as the particle, interacting with an envi-

ronment that constitutes a heat bath. In the present case of a solid, the particle degree of freedom represents that of the electron and the ionic lattice degrees of freedom that of the heat bath. The Hamiltonian for such a system has the form

$$\hat{H} = \hat{H}_0 + \hat{H}_i, \quad (2.1)$$

where the Hamiltonian for the noninteracting subsystems

$$\hat{H}_0 = \hat{H}_p + \hat{H}_B \quad (2.2)$$

consists of a term \hat{H}_p describing the particle and a term \hat{H}_B the heat bath. A heat bath can quite generally be modeled (Feynman and Vernon, 1963; Caldeira and Leggett, 1983) by a set of harmonic-oscillator degrees of freedom represented by the position and momentum operators \hat{x}_q and \hat{p}_q labeled by q ,

$$\hat{H}_B = \sum_q \left[\frac{\hat{p}_q^2}{2M_q} + \frac{1}{2} M_q \omega_q^2 \hat{x}_q^2 \right], \quad (2.3)$$

The oscillators are characterized by their mass M_q and frequency ω_q and in the considered case describe the lattice vibrations.

Bearing in mind the particle degree of freedom representing an electron in a solid, subject to an external classical force F , for the particle Hamiltonian we choose

$$\hat{H}_p = \frac{\hat{p}^2}{2m} - F\hat{x}. \quad (2.4)$$

Here, m is the mass of the electron, and \hat{x} and \hat{p} are the position and momentum operators for the particle, respectively.¹ We have above chosen the external force to be spatially homogeneous and time independent. The method presented in the following may be straightforwardly extended to arbitrary external forces.

When the lattice vibrations of the crystalline solid of volume V is the realization of the heat bath, the interaction part has the standard normal-mode expansion form

$$\hat{H}_i = \frac{i}{\sqrt{V}} \sum_q (g_q e^{iq\hat{x}} \hat{a}_q - g_q^* e^{-iq\hat{x}} \hat{a}_q^\dagger), \quad (2.5)$$

where \hat{a}_q^\dagger and \hat{a}_q are creation and annihilation operators for the normal modes of the lattice vibrations

$$\hat{a}_q = \frac{i}{\sqrt{2M\hbar\omega_q}} (\hat{p}_q - iM\omega_q \hat{x}_q), \quad (2.6)$$

\hat{a}_q^\dagger is the Hermitian conjugate, and $*$ denotes complex conjugation. The ionic mass is denoted by M , and g_q is the coupling constant for the q th mode.

The normal-mode representation of the bath Hamiltonian has the standard form

$$\hat{H}_B = \sum_q \hbar\omega_q (\hat{a}_q^\dagger \hat{a}_q + \frac{1}{2}). \quad (2.7)$$

¹For simplicity we have at this point chosen a one-dimensional notation since the description is trivially generalizable to arbitrary dimensions.

After presenting the model for the physical system, an electron in a solid interacting with the vibrations of the lattice and acted upon by an external force, we turn to studying the quantum dynamics of the model.

In quantum-statistical mechanics, the averaging necessary when only partial information is available leads directly to a description of the statistical ensemble of quantum-mechanical systems in terms of the statistical operator $\hat{\rho}$, which is a Hermitian operator whose trace (sum of diagonal matrix elements) equals one (Landau and Lifshitz, 1980). The diagonal matrix elements of the statistical operator represent the probability that a measurement will reveal the number corresponding to the quantum state in question; moreover, any expectation value of a physical quantity is expressible in terms of the statistical operator.

The Schrödinger equation governing the temporal evolution of a quantum state leads to the following temporal evolution of the statistical operator determined by the Liouville-von Neumann equation:

$$\hbar \frac{d\hat{\rho}}{dt} = -i[\hat{H}, \hat{\rho}] . \quad (2.8)$$

Here, $[,]$ denotes the commutator.

The formal solution of the Liouville-von Neumann equation is given in terms of the evolution operator \hat{U} of the system

$$\hat{\rho}(t) = \hat{U}(t, t_i) \hat{\rho}(t_i) \hat{U}^\dagger(t, t_i) , \quad (2.9)$$

the evolution operator is specified in terms of the Hamiltonian

$$\hat{U}(t, t') = \exp \left[-\frac{i}{\hbar} \hat{H}(t - t') \right] , \quad (2.10)$$

and $\hat{\rho}(t_i)$ is the statistical operator at some initial time t_i .

Since the degrees of freedom, other than that of the particle, are considered as representing a heat bath, they are left unobserved, and we are only interested in the measurable properties of the particle.² This is the situation pertaining to the measurement of electrical conductivity which we have in mind. We must therefore perform the trace over the bath degrees of freedom, that is, allow for all possible final states of the bath, and are led to study the reduced statistical operator \hat{f} for the particle

$$\hat{f}(t) = \text{tr} \hat{\rho}(t) , \quad (2.11)$$

where tr denotes the trace over the bath degrees of freedom. All physical properties pertaining to the particle can be expressed in terms of the reduced statistical opera-

tor. As an example, the expectation value of the current density j of the particle at time t is given by the expression

$$j(x, t) = \frac{e\hbar}{2mi} \left[\frac{\partial}{\partial x} - \frac{\partial}{\partial x'} \right] f(x, x', t) |_{x'=x} , \quad (2.12)$$

where e denotes the electronic charge, and the reduced density matrix in the spatial or x representation, $f(x, x', t)$, is given by

$$f(x, x', t) = \text{tr} \langle x | \hat{\rho}(t) | x' \rangle . \quad (2.13)$$

Having described the model for a particle interacting with lattice vibrations, we now turn to the Feynman diagrammatics for the reduced density matrix.

B. Feynman diagrammatics for the reduced density matrix

In this subsection we are not so much interested in transient properties as in properties of stationary states, and we shall therefore assume that at some initial time t_i the statistical operator is separable,

$$\hat{\rho}(t_i) = \hat{f}(t_i) \hat{\rho}_B , \quad (2.14)$$

and that the bath degrees of freedom are in thermal equilibrium at the temperature T , so that initially the statistical operator for the bath is given by

$$\hat{\rho}_B = \frac{\exp(-\hat{H}_B/k_B T)}{\text{tr}[\exp(-\hat{H}_B/k_B T)]} . \quad (2.15)$$

Subsequent to the initial time the two subsystems are allowed to interact, and the dynamics of the particle is described by the reduced density matrix, which, according to Eq. (2.13), is given by the expression³

$$f(x, x', t) = \int d\bar{x} \int d\bar{x}' J(x, x', t; \bar{x}, \bar{x}', t_i) f_i(\bar{x}, \bar{x}') , \quad (2.16)$$

where J , the propagator of the reduced density matrix, according to Eq. (2.9) is determined by

$$\begin{aligned} J(x, x', t; \bar{x}, \bar{x}', t_i) &= \text{tr}[\hat{\rho}_B \langle \bar{x}' | \hat{U}^\dagger(t, t_i) | x' \rangle \langle x | \hat{U}(t, t_i) | \bar{x} \rangle] , \\ & \quad (2.17) \end{aligned}$$

and the initial reduced density matrix is the matrix element

$$f_i(\bar{x}, \bar{x}') = \langle \bar{x} | \hat{f}(t_i) | \bar{x}' \rangle . \quad (2.18)$$

²In cases where nonequilibrium states of the lattice degrees of freedom need to be considered (as, for instance, in the case of the phonon-drag effect), we must in addition introduce the reduced density matrices for these degrees of freedom, which in turn leads to a set of equations coupling the density matrices of all the degrees of freedom.

³We note that we of course include all transient effects of the chosen initial condition, Eqs. (2.14) and (2.15). Whether this choice is appropriate for the study of transient effects depends on the given physical situation.

We shall be interested in the perturbative structure, in the coupling to the environment, of the density matrix, and shall therefore express the evolution operator in the interaction picture with respect to \hat{H}_0

$$\hat{U}(t, t') = \exp \left[-\frac{i}{\hbar} \hat{H}_0 t \right] T \exp \left[-\frac{i}{\hbar} \int_{t'}^t d\bar{t} \hat{H}_i(\bar{t}) \right] \times \exp \left[\frac{i}{\hbar} \hat{H}_0 t' \right], \quad (2.19)$$

$$f(x, x', t) = \int d\bar{x} \int d\bar{x}' \int dx_1 \int dx_2 \int dx'_1 \int dx'_2 \times \text{tr} \left[\hat{\rho}_B(\bar{x}') \left| \exp \left[-\frac{i}{\hbar} \hat{H}_p t_i \right] \right| x'_1 \right] \langle x'_1 | \tilde{T} \exp \left[\frac{i}{\hbar} \int_{t_i}^t d\bar{t} \hat{H}_i(\bar{t}) \right] | x'_2 \rangle \langle x'_2 | \exp \left[\frac{i}{\hbar} \hat{H}_p t \right] | x' \rangle f_i(\bar{x}, \bar{x}') \times \langle x | \exp \left[-\frac{i}{\hbar} \hat{H}_p t \right] | x_1 \rangle \langle x_1 | T \exp \left[-\frac{i}{\hbar} \int_{t_i}^t d\bar{t} \hat{H}_i(\bar{t}) \right] | x_2 \rangle \langle x_2 | \exp \left[\frac{i}{\hbar} \hat{H}_p t_i \right] | \bar{x} \rangle. \quad (2.21)$$

Here, \tilde{T} denotes the anti-time-ordering operation.

To obtain a diagrammatic expansion, we introduce an iterative solution for the evolution operator, that is, we expand the time-ordered and anti-time-ordered exponentials, e.g.,

$$T \exp \left[-\frac{i}{\hbar} \int_{t_i}^t d\bar{t} \hat{H}_i(\bar{t}) \right] = \sum_{n=0}^{\infty} \frac{(-i)^n}{\hbar^n} \int_{t_i}^t dt_n \cdots \int_{t_i}^{t_2} dt_1 \hat{H}_i(t_n) \cdots \hat{H}_i(t_1). \quad (2.22)$$

We then insert complete sets of particle eigenstates,

$$1 = \int dx |x, t\rangle \langle x, t|, \quad (2.23)$$

where $\{|x, t\rangle\}_{x \in R}$ is the complete set of eigenstates for the position operator in the interaction representation $x(t)$, that is,

$$\hat{x}(t)|x, t\rangle = x|x, t\rangle. \quad (2.24)$$

We obtain products of terms of the form

$$\langle x_3, t_3 | \hat{H}_i(t_2) | x_2, t_2 \rangle = \frac{i}{\sqrt{V}} \sum_q [g_q(x_2) \hat{a}_q(t_2) - \text{H.c.}] \langle x_3, t_3 | x_2, t_2 \rangle, \quad (2.25)$$

$$\langle x | \hat{U}(t, t_i) | \bar{x} \rangle = \sum_{n=0}^{\infty} \frac{i^n}{\hbar^n} \int_{t_i}^t dt_n \cdots \int_{t_i}^{t_1} dt_1 \int dx_n \cdots \int dx_1$$

$$\times V^{-n/2} G^R(x, t; x_n, t_n) G^R(x_n, t_n; x_{n-1}, t_{n-1}) \cdots G^R(x_1, t_1; \bar{x}, t_i) \times \sum_{q_1, \dots, q_n} \{ [g_{q_n}(x_n) \hat{a}_{q_n}(t_n) - \text{H.c.}] \cdots [g_{q_1}(x_1) \hat{a}_{q_1}(t_1) - \text{H.c.}] \}, \quad (2.30)$$

where

$$\hat{H}_i(t) = \exp \left[\frac{i}{\hbar} \hat{H}_0 t \right] \hat{H}_i \exp \left[-\frac{i}{\hbar} \hat{H}_0 t \right] \quad (2.20)$$

describes the interaction term in the interaction representation and T denotes the time-ordering operation necessary due to the non-commutativity of the operators. Inserting complete sets of particle states on the right-hand side of Eq. (2.16), we obtain for the reduced density matrix

where $\hat{a}_q(t)$ is the annihilation operator in the interaction representation

$$\hat{a}_q(t) = \exp \left[\frac{i}{\hbar} \hat{H}_B t \right] \hat{a}_q \exp \left[-\frac{i}{\hbar} \hat{H}_B t \right], \quad (2.26)$$

and H.c. stands for Hermitian conjugate. The matrix element $\langle x_3, t_3 | x_2, t_2 \rangle$ is the quantum-mechanical amplitude for propagation of the particle between space-time points

$$\langle x, t | x', t' \rangle = \langle x | \exp \left[-\frac{i}{\hbar} H_p(t-t') \right] | x' \rangle, \quad (2.27)$$

and $g_q(x)$ is the coupling function

$$g_q(x) = g_q e^{iqx}. \quad (2.28)$$

The time-ordering restriction on the integration limits in Eq. (2.22), demanded by the time-ordering operation, can be lifted by introducing the step function θ , resulting in the appearance of the retarded Green's function for the particle

$$G^R(x, t; x', t') = -i\theta(t-t') \langle x, t | x', t' \rangle. \quad (2.29)$$

For the matrix element of interest, we then obtain

which has the typical structure of a product of propagators with interactions occurring at intermediate space-time points, labeling the various alternatives or intermediate states.

For the anti-time-ordered exponential we obtain a similar expression, the difference being that the advanced Green's function G^A appears instead of the retarded

$$G^A(x, t; x', t') = [G^R(x', t'; x, t)]^* . \quad (2.31)$$

The only operation left to perform in Eq. (2.21) is then the trace over the bath states, which can be accomplished by the following procedure. For any order in perturbation theory, we have in Eq. (2.21) a corresponding string S of bath operators which are explicitly time ordered or anti time ordered,

$$S = \text{tr} \{ \hat{\rho}_B \tilde{T} [\hat{c}_{q_n}(\tilde{t}_n) \cdots \hat{c}_{q_1}(\tilde{t}_1)] \times T [\hat{c}_{q_m}(t_m) \cdots \hat{c}_{q_1}(t_1)] \} , \quad (2.32)$$

where \hat{c}_q denotes either a creation or an annihilation operator for the normal modes of the lattice vibrations. This expression is most easily evaluated by introducing the closed-contour description. Consider the time-ordered and anti-time-ordered times as lying on a pair of different real axes—the time-ordered ones on a forward and the anti-time-ordered ones, distinguished by a tilde, on the return part of a closed contour c_i starting and ending at t_i , as depicted in Fig. 1. Equation (2.32) can then be subsumed under one contour ordering along the contour c_i ,

$$S = \text{tr} \{ \hat{\rho}_B T_{c_i} [\hat{c}_{q_n}(\tilde{t}_n) \cdots \hat{c}_{q_1}(\tilde{t}_1) \hat{c}_{q_m}(t_m) \cdots \hat{c}_{q_1}(t_1)] \} , \quad (2.33)$$

where T_{c_i} orders the operators according to their position on the contour c_i (earliest positions to the right). Such an expression can be decomposed according to the statistical Wick's theorem, which relies only on the simple property

$$[\hat{c}_q, \hat{\rho}_B] = \hat{\rho}_B \hat{c}_q [\exp(\lambda_c \hbar \omega_q / k_B T) - 1] , \quad (2.34)$$

valid for a quadratic bath Hamiltonian ($\lambda_c = \pm 1$, depending upon whether c_q is a creation or an annihilation operator). Using this property, by moving creation operators to the right, one obtains for Eq. (2.33) a sum over paired products

$$S = \sum_{\text{a.p.p.}} \prod_{q, q'} \langle T_{c_i} [\hat{c}_q(\tau) \hat{c}_{q'}(\tau')] \rangle , \quad (2.35)$$

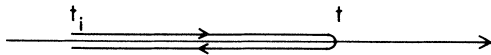


FIG. 1. The closed-time-path contour.

where the sum is over all possible ways of picking pairs (a.p.p.) among the $n + m$ operators⁴ and where

$$\langle T_{c_i} [\hat{c}_q(\tau) \hat{c}_{q'}(\tau')] \rangle = \text{tr} (\hat{\rho}_B T_{c_i} [\hat{c}_q(\tau) \hat{c}_{q'}(\tau')]) \quad (2.36)$$

defines the bracket as the weighted average with respect to the equilibrium bath state, with τ and τ' being arbitrary times on the contour c_i . So, for example (we suppress, for the present consideration, the immaterial q labels),

$$\begin{aligned} & \text{tr} (\hat{\rho}_B T_{c_i} [a(\tau_1) a^\dagger(\tau_2) a(\tau_3) a^\dagger(\tau_4)]) \\ &= \langle T_{c_i} [a(\tau_1) a^\dagger(\tau_2)] \rangle \langle T_{c_i} [a(\tau_3) a^\dagger(\tau_4)] \rangle \\ &+ \langle T_{c_i} [a(\tau_1) a^\dagger(\tau_4)] \rangle \langle T_{c_i} [a(\tau_3) a^\dagger(\tau_2)] \rangle . \end{aligned} \quad (2.37)$$

Detailed proofs of Wick's theorem, Eq. (2.35), exist in a multitude of forms in the literature. We shall not, therefore, repeat them here, but refer the reader to the elegant and simple proof of Mills (1969). Performing the trace over the bath states in Eq. (2.21) therefore corresponds to pairing the interaction points in all possible ways.

We can now state the Feynman diagrammatics for the reduced density matrix in the spatial representation: The Feynman diagrams for the reduced density matrix f comprise all the topologically different diagrams of the type depicted in Fig. 2 (showing only the lowest-order terms). The reduced density matrix, being a single-time object, is represented as vertical, and the identifying mark of the single-particle approach, that the retarded and advanced particle lines are separated by the initial reduced density matrix, is displayed.

The diagrams are transcribed according to the following Feynman rules:

The stipulated vertical line represents the reduced density matrix,

$$\begin{array}{c} \bullet \\ | \\ x \\ | \\ x' \\ | \\ \bullet \end{array} = f(x, x', t) . \quad (2.38)$$

An upper solid line represents the retarded-particle Green's function,

$$\begin{array}{c} \bullet \\ \xrightarrow{R} \\ x \quad t \end{array} \begin{array}{c} \bullet \\ \xleftarrow{R} \\ x' \quad t' \end{array} = G^R(x, t; x', t') . \quad (2.39)$$

A lower solid line represents the advanced-particle Green's function,

$$\begin{array}{c} \bullet \\ \xrightarrow{A} \\ x \quad t \end{array} \begin{array}{c} \bullet \\ \xleftarrow{A} \\ x' \quad t' \end{array} = G^A(x', t'; x, t) . \quad (2.40)$$

⁴If $n + m$ is odd, the expression for S equals zero, since the expectation value is with respect to the quadratic bath Hamiltonian.

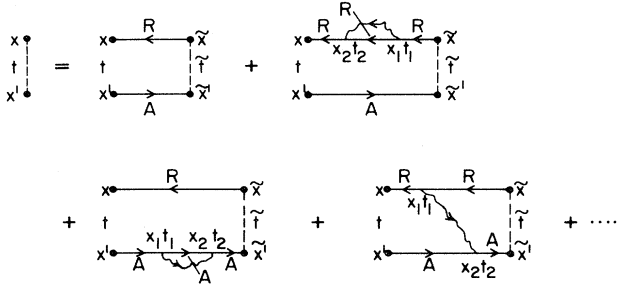


FIG. 2. The Feynman diagrams for the reduced density matrix.

A wavy line represents the phonon propagator,

$$\begin{matrix} \text{wavy line} \\ \text{---} \end{matrix} = D(x, t; x', t'). \tag{2.41}$$

In accordance with the derivation, integration over internal space-time points should be performed.

With the chosen convention (as illustrated in Fig. 2) for assigning direction to the phonon line, we need only introduce one type of phonon propagator, the so-called “greater” phonon propagator:

$$\begin{aligned} D(x, t; x', t') &= D^>(x, t; x', t') \\ &= \frac{-i}{V\hbar^2} \sum_{qq'} \langle [g_q(x)\hat{a}_q(t) - \text{H.c.}] \\ &\quad \times [g_{q'}(x')\hat{a}_{q'}(t') - \text{H.c.}] \rangle. \end{aligned} \tag{2.42}$$

The different convention in which the arrow on the phonon line is opposite to the one chosen in Fig. 2 would necessitate the introduction of the “lesser” propagator:

$$D^<(x, t; x', t') = D^>(x', t'; x, t). \tag{2.43}$$

The convention of distinguishing times on the backward part of the contour by a tilde is now superfluous and will henceforth be omitted.

The reason for the absence of an explicitly time-ordered phonon propagator in the theory, as the Wick decomposition, Eq.(2.35), suggests, is that we are dealing with only one particle (besides the oscillator bath), so that no particle-hole (pair) creation can take place as in the many-body case. This diagrammatic structure of the density matrix is closely related to the diagrammatic structure of, for example, the fermionic Keldysh Green’s function (or the so-called lesser Green’s function) in the many-body problem (Kadanoff and Baym, 1962), except for the above-mentioned one-particle feature. In the many-body problem additional retarded and advanced phonon propagators would appear in accordance with the possibility of creation of particle-hole pairs.

The final ingredient needed to turn a diagram for the reduced density matrix into an analytical expression is a knowledge of the particular analytical form of the Green’s functions and propagators for the problem in

question. Again, the one-particle feature allows us to assert these in elementary quantum-mechanical terms. As can be seen from the definition (2.29), the retarded-particle Green’s function, $G^R(x, t; x', t')$, is nothing but the solution of the one-particle Schrödinger equation

$$i\hbar \frac{\partial \psi}{\partial t} = H_p \psi, \tag{2.44}$$

at times t later than t' , for the given initial condition that at time t' the particle be prepared in a state of definite position x' ,

$$\lim_{t \rightarrow t'} \psi(x, t) = \delta(x - x'), \tag{2.45}$$

while prior to time t' it be absent in accordance with the presence of the step function in the definition, Eq. (2.29).

The phonon propagator of Eq. (2.42) is readily calculated, since it involves only an equilibrium average with respect to the bath state. For compactness in notation, we include the particle-phonon coupling constant g_q in the definition of the phonon propagator, so that the analytical expression following from Eq. (2.42) is

$$D(x, t; x', t') = \frac{1}{V} \sum_q \exp \left[\frac{i}{\hbar} q(x - x') \right] D_q(t, t'), \tag{2.46}$$

with the Fourier component

$$\begin{aligned} D_q(t, t') &= \frac{i}{\hbar^2} |g_q|^2 [(1 + n_q) e^{-i\omega_q(t-t')} \\ &\quad + n_{-q} e^{i\omega_{-q}(t-t')}] . \end{aligned} \tag{2.47}$$

Here, n denotes the Bose function.

The double time diagrams of Fig. 2 for the density matrix are generic to quantum-statistical mechanics. The diagonal elements of the density matrix, which are real numbers, are expressed as sums of complex numbers, but they come in pairs that are each other’s complex conjugate’s as is characteristic of quantum-mechanical interference. In this single-particle approach the quantum-mechanical interference aspect of electronic motion is directly displayed, and we shall exploit this feature, demonstrating that the Feynman diagrammatics give a useful physical picture of quantum transport.

C. Temporal evolution on differential form of the reduced density matrix and the corresponding diagrammatic representation

In the preceding section, we examined the time evolution of the reduced density matrix in integral form and described the diagrammatic expansion in the spatial representation. In the next section we shall take the kinetic approach, which amounts to studying the differential time evolution of the reduced density matrix. This will permit us to eliminate the initial density matrix and thereby pave the way for describing the steady-state situ-

ation, so important to transport theory, as is well known from the Boltzmann description.

In order to do this, we now display the spatial representation of the Liouville–von Neumann equation for the reduced density matrix, and interpret it diagrammatically. This means that we must look at the change in time of the reduced density matrix. From Eq. (2.8) we obtain, by employing Eq. (2.19) and taking the trace over the bath degrees of freedom,

$$\hbar \frac{\partial \hat{f}}{\partial t} = -i[\hat{H}_p, \hat{f}(t)] - i \text{tr} \{ [\hat{H}_i(t), \hat{\rho}(t)] \}. \quad (2.48)$$

The spatial representation of the operator equation (2.48) leads to the following equation for the reduced density matrix:

$$\frac{\partial f(x, x', t)}{\partial t} - \frac{i}{\hbar} \langle x | [\hat{f}(t), \hat{H}_p] | x' \rangle = -iF[f_i], \quad (2.49)$$

where F is a functional of the reduced density matrix at the initial time (suppressing the parametrical dependence on x, x' , and t):

$$\begin{aligned} F[f_i] = & -\frac{1}{\hbar} \int d\bar{x} \int d\bar{x}' \text{tr} \left[\hat{\rho}_B \left\langle \bar{x}' \left| \exp \left[-\frac{i}{\hbar} \hat{H}_p t_i \right] \tilde{T} \exp \left[\frac{i}{\hbar} \int_{t_i}^t d\bar{t} \hat{H}_i(\bar{t}) \right] \right. \right. \\ & \left. \left. \times \exp \left[\frac{i}{\hbar} \hat{H}_p t \right] \right| x' \right\rangle \hat{H}_i(x', \{ \hat{x}_q(t), \hat{p}_q(t) \}_q) f_i(\bar{x}, \bar{x}') \langle x | \hat{U}(t, t_i) | \bar{x} \rangle \right] \\ & + \frac{1}{\hbar} \int d\bar{x} \int d\bar{x}' \text{tr} \left[\hat{\rho}_B \langle \bar{x}' | \hat{U}^\dagger(t, t_i) | x' \rangle \hat{H}_i(x, \{ \hat{x}_q(t), \hat{p}_q(t) \}_q) \right. \\ & \left. \times \langle x | \exp \left[-\frac{i}{\hbar} \hat{H}_p t \right] T \exp \left[-\frac{i}{\hbar} \int_{t_i}^t d\bar{t} \hat{H}_i(\bar{t}) \right] \exp \left[\frac{i}{\hbar} \hat{H}_p t_i \right] \right| \bar{x} \rangle f_i(\bar{x}, \bar{x}') \right]. \quad (2.50) \end{aligned}$$

The operator in the interaction picture $\hat{H}_i(x, \{ \hat{x}_q(t), \hat{p}_q(t) \}_q)$ is now only an operator with respect to the bath degrees of freedom and has the explicit form

$$\begin{aligned} \hat{H}_i(x, \{ \hat{x}_q(t), \hat{p}_q(t) \}_q) = & \frac{i}{\sqrt{V}} \sum_q [g_q e^{iqx} \hat{a}_q(t) \\ & - g_q^* e^{-iqx} \hat{a}_q^\dagger(t)]. \quad (2.51) \end{aligned}$$

The functional F has, according to Eqs. (2.50) and (2.21), a diagrammatic representation obtained from the diagrams for the reduced density matrix f by the following prescription: Remove the external retarded particle line or the external advanced one. The functional F thus has the diagrammatic structure shown in Fig. 3, where the box signifies that we can have arbitrary entanglements of phonon lines. A conventional minus sign has been inserted for diagrams in which the initial phonon line begins on the lower line. A typical diagram for the functional F , containing three phonon lines, thus has the form shown in Fig. 4.

For problems that are not concerned with transient behavior, such as nonequilibrium steady-state problems, it would be preferable to have a representation in which the initial condition does not appear explicitly. Such a formulation is provided by introducing the concept of ir-

reducibility. A diagram is reducible if it can be cut in two by cutting only two electron lines. Using this concept, we can now eliminate the explicit appearance of the initial-time reduced density matrix f_i by observing the following resummation of diagrams: Take an arbitrary diagram from the expansion of F , say, the one depicted in Fig. 4. It is by construction reducible. Move back in time along the particles lines to the first time t_1 , where the diagram can be cut in two by cutting only the particle lines, as illustrated in Fig. 4. At times prior to t_1 , any process, that is, appearance of phonon lines, can take place and can be imagined as one of all the possible diagrams not depicted. The total sum of processes prior to t_1 is thus the same as the sum of processes for the density matrix at time t_1 , so that in the process the initial-time density matrix f_i is propagated to time t_1 . This argument demonstrates the identity

$$F[f_i] = \tilde{F}[f], \quad (2.52)$$

where \tilde{F} is the functional

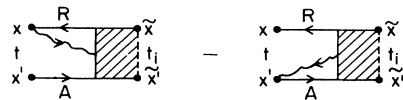


FIG. 3. Diagrammatic representation of the functional F .

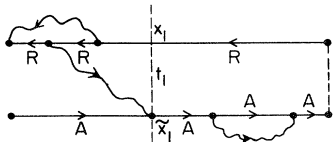


FIG. 4. Typical three-phonon line diagram for F .

$$\bar{F}[f] = \int dx_1 \int dx'_1 \int_{t_i}^t dt_1 \bar{J}(x, x', t; x_1, x'_1, t_1) \times f(x_1, x'_1, t_1), \tag{2.53}$$

and where the diagrammatic expansion of \bar{J} , the “irreducible” reduced density-matrix propagator, consists of all irreducible diagrams, of which the lowest-order ones are shown in Fig. 5. We note that irreducibility of a diagram is determined not by topology alone, but also by the relative time ordering between times on the upper and lower branches. This feature, which distinguishes the present diagram technique from the many-body technique, is the result of dealing with a single-time object such as a density matrix.

Instead of pursuing the general discussion at this point, and in order to gain familiarity with the Feynman rules and the general features of the method, let us look at the lowest-order contribution to the irreducible propagator \bar{J} . This contribution is depicted by the four diagrams in Fig. 5. We observe that for all lowest-order diagrams, irreducibility is trivial. As illustration, we note that the first diagram in Fig. 5 corresponds to the analytical expression $\bar{J}^{(1)}$ given by

$$\bar{J}^{(1)} = G^R(x, t; \bar{x}, \bar{t}) G^A(\bar{x}', \bar{t}; x', t) D(x, t; \bar{x}, \bar{t}), \tag{2.54}$$

by application of the Feynman rules. The full calculation of the lowest-order irreducible propagator will be deferred to the next section, where the kinetic approach to transport is considered.

Up to this point we have stressed the spatial representation. Besides providing a very useful pictorial representation of quantum transport, it also allows proper inclusion of boundary conditions, thus making it applicable to the description of a general, inhomogeneous, situation. The general formalism presented is therefore of importance for a full quantum-statistical description of physical systems of finite size, a feature we shall take advantage of in the later discussion of mesoscopic phenomena.

III. THE KINETIC APPROACH

In this section, we shall consider a treatment of quantum transport that resembles the kinetic description of

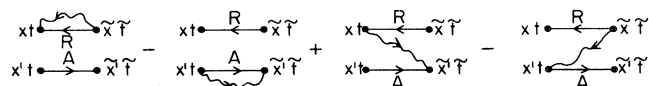


FIG. 5. Lowest-order diagrams contributing to the irreducible propagator \bar{J} .

the dynamics of classical gases due to Boltzmann (1872). The virtues of a transport description in terms of kinetic equations are (1) the simple physical interpretation it can produce and (2) its ability to describe nonlinear behavior. Furthermore, it allows a straightforward description of thermal properties, such as heat conduction, whereas a treatment of nonmechanical induced nonequilibrium states in linear-response theory is more complex.

A. The Wigner function

The central object to the Boltzmann approach to nonequilibrium classical statistical mechanics is the one-particle probability distribution function over phase space. In quantum mechanics the Heisenberg uncertainty principle excludes the existence of a probability distribution function with such a physical interpretation, but not, however, the introduction of a function with a formal resemblance to it. This so-called Wigner function (Wigner, 1932) is definable in terms of the (reduced) density matrix by Fourier transformation with respect to the relative spatial coordinate

$$f(p, R, t) = \int dr \exp\left[-\frac{i}{\hbar} pr\right] f\left(R + \frac{1}{2}r, R - \frac{1}{2}r, t\right). \tag{3.1}$$

For a spatially homogeneous state (that is, one for which f is independent of R), the Wigner function is identical to the momentum distribution function, and for a spatially localized state (f independent of p), it is identical with the density distribution function.⁵ Furthermore, in the classical limit, where all relevant actions are huge compared to Planck’s constant, the Wigner function reduces to the Boltzmann distribution function. However, caution must be exercised in interpreting the Wigner function in a probabilistic sense. Although the Wigner function is always a real function, there is no general physical principle guaranteeing that it be non-negative. In any event, the Wigner function is a valid construction, and all physical quantities are expressible in terms of it. For instance, for the previously introduced current density we have, in terms of the Wigner function,

$$j(R, t) = \frac{e}{m} \int \frac{dp}{2\pi\hbar} pf(p, R, t). \tag{3.2}$$

The integro-differential equation for the density matrix, Eq. (2.49), can be turned into an equation for the Wigner function by Fourier transformation,

⁵This is simply a restatement of the fact that only the diagonal elements of the density matrix have a physical interpretation, here for the cases of momentum and spatial representations, respectively.

$$\begin{aligned} & \frac{\partial f(p, R, t)}{\partial t} + F \frac{\partial f(p, R, t)}{\partial p} \\ &= \int \frac{d\tilde{p}}{2\pi\hbar} \int d\tilde{R} \int_{i_1}^t d\tilde{t} \tilde{J}(p, R, t; \tilde{p}, \tilde{R}, \tilde{t}) f(\tilde{p}, \tilde{R}, \tilde{t}), \end{aligned} \quad (3.3)$$

where the irreducible propagator \tilde{J} in the Wigner or mixed representation is

$$\begin{aligned} & \tilde{J}(p, R, t; \tilde{p}, \tilde{R}, \tilde{t}) \\ &= \int dr \int d\tilde{r} \exp \left[-\frac{i}{\hbar} pr + \frac{i}{\hbar} \tilde{p}\tilde{r} \right] \\ & \quad \times \tilde{J}(R + \frac{1}{2}r, R - \frac{1}{2}r, t; \tilde{R} + \frac{1}{2}\tilde{r}, \tilde{R} - \frac{1}{2}\tilde{r}, \tilde{t}), \end{aligned} \quad (3.4)$$

and the second term on the left-hand side of Eq. (2.49) reduces to the usual driving term of the Boltzmann equation in the case of a spatially uniform external force. Each diagram for the irreducible propagator in the spatial representation can, by simply Fourier transforming, be labeled in the Wigner representation.

A diagrammatic technique is only useful for calculational purposes if the structure has easily recognizable features to ensure that fundamental properties of physical quantities are respected. For example, what in the diagrammatic structure reflects the property that the Wigner function is a real function? As we shall see shortly, it is an easily recognizable symmetry between diagrams of the irreducible propagator \tilde{J} . For any diagram $\tilde{J}^d(x, x', t; \tilde{x}, \tilde{x}', \tilde{t})$ of \tilde{J} , labeled by its external points, there is a symmetric one $\tilde{J}^{\bar{d}}(x, x', t; \tilde{x}, \tilde{x}', \tilde{t})$ obtained by mirror reflection of the phonon lines in a line that is parallel to the upper and lower lines and in between them. The general structure of the diagrams, as displayed in Fig. 3 clearly allows for such a symmetry operation. Figure 5 is an example containing two such pairs of mirror diagrams. Exploiting the relationship between the retarded and advanced Green's functions, Eq. (2.31), and the properties

$$[D^{\bar{z}}(x, t; x', t')]^* = -D^z(x', t'; x, t), \quad (3.5)$$

it follows, with the conventional minus sign as introduced in Fig. 3, that

$$[\tilde{J}^d(x, x', t; \tilde{x}, \tilde{x}', \tilde{t})]^* = \tilde{J}^{\bar{d}}(x, x', t; \tilde{x}, \tilde{x}', \tilde{t}). \quad (3.6)$$

Transforming to the mixed or Wigner representation, we therefore have the property

$$[\tilde{J}^d(p, R, t; \tilde{p}, \tilde{R}, \tilde{t})]^* = \tilde{J}^{\bar{d}}(p, R, t; \tilde{p}, \tilde{R}, \tilde{t}). \quad (3.7)$$

The fact that the Wigner function is real is thus reflected in the diagrammatic structure by the two symmetric classes the diagrams fall into, as allowed in general by the two classes of Fig. 3.

B. The intracollisional field effect for electron-phonon interaction

As an example of the usefulness of the kinetic approach, we shall in this section study the time evolution of the density matrix or, equivalently, the Wigner function in the weak-coupling limit; that is, the coupling to the heat bath is treated to lowest order. Since this is the only limitation imposed, we are treating the effect of the external field completely, and we shall see that the so-called intracollisional field effect is quite simply incorporated.

The irreducible propagator in the weak-coupling limit is given by the diagrams depicted in Fig. 5. The retarded and advanced Green's functions include the external field, as is evident in Eq. (2.21). The retarded Green's function $G^R(x, t; x', t')$, represented by a line in the diagram in Fig. 5 and defined in Eq. (2.29) describes the propagation of a particle created at space-time point (x', t') , this being the information content of Eqs. (2.44) and (2.45).

This information is compactly combined in the Green's-function-type equation

$$\left[i\hbar \frac{\partial}{\partial t} - H_p \right] G^R(x, t; x', t') = \hbar \delta(x - x') \delta(t - t'), \quad (3.8)$$

$$G^R(x, t; x', t') = 0 \text{ for } t < t', \quad (3.9)$$

where the particle Hamiltonian, Eq. (2.4), in the position representation is

$$H_p = -\frac{\hbar^2}{2m} \frac{d^2}{dx^2} - Fx. \quad (3.10)$$

The particle propagator, the Green's function, can be obtained by solving the differential equation directly or by simply recalling that for quadratic Hamiltonians the propagator is given, up to a prefactor determined by the initial condition, in terms of the classical action

$$\begin{aligned} G^R(x, t; x', t') &= -i\theta(t - t') \left[\frac{m}{2\pi i\hbar(t - t')} \right]^{1/2} \\ & \quad \times \exp \left[\frac{i}{\hbar} S(x, t; x', t') \right], \end{aligned} \quad (3.11)$$

where the classical action

$$S(x, t; x', t') = \int_{t'}^t dt \left\{ \frac{1}{2}m[\dot{x}(t)]^2 + Fx(t) \right\} \quad (3.12)$$

is evaluated for the classical path $x(t)$ with start and end points x' and x , that is, the solution of the problem

$$m \frac{d^2 x}{dt^2} = F, \quad x(t') = x', \quad x(t) = x. \quad (3.13)$$

Inserting the solution of Eq. (3.13), we obtain for the classical action

$$S(x, t; x', t') = \frac{m(x - x')^2}{2(t - t')} + \frac{1}{2} F(t - t')(x + x') - \frac{F^2(t - t')^3}{24m}. \quad (3.14)$$

As dictated by the introduction of the Wigner representation, we need the propagator in this representation (obtainable by a simple Fourier transformation),

$$G_p^R(R, t, t') = \int dr \exp \left[-\frac{i}{\hbar} pr \right] G^R(R, r, t, t') = -i\theta(t - t') \exp \left[-\frac{i}{\hbar} \left[\epsilon(p)(t - t') + \frac{F^2(t - t')^3}{24m} - FR(t - t') \right] \right], \quad (3.15)$$

where we have introduced the single-particle energy $\epsilon(p)$,

$$\epsilon(p) = \frac{p^2}{2m}. \quad (3.16)$$

With all the necessary ingredients explicitly at hand, we can now evaluate the irreducible propagator. We start by calculating the contribution from the diagram depicted in Fig. 6. Let us assume that we start from a spatially homogeneous state (if this is not the case, we must examine the spatial extension of the irreducible

propagator \tilde{J}). The Wigner function will then be independent of its spatial coordinate, and, along with the integration over r and \tilde{r} , we can perform the integration over \tilde{R} [as a consequence of which the right-hand side of Eq. (3.3), or specifically $\int d\tilde{R} \tilde{J}(p, R, t; \tilde{p}, \tilde{R}, \tilde{t})$, becomes independent of R].

Introducing the Fourier expansion for the propagators G^R , G^A , and D appearing in Fig. 6, we are able to carry out the resulting integrations, and we obtain for this diagram the following contribution to the right-hand side of Eq. (3.3):

$$I_{\text{in}}^{(1)}[f] = 2 \int_{t_i}^t d\tilde{t} \int \frac{dp'}{2\pi\hbar} D_{p-p'}(t, \tilde{t}) f(p' - \frac{1}{2}F(t - \tilde{t}), \tilde{t}) \exp \left[-\frac{i(t - \tilde{t})}{\hbar} [\epsilon(p' - \frac{1}{2}F(t - \tilde{t})) - \epsilon(p - \frac{1}{2}F(t - \tilde{t}))] \right]. \quad (3.17)$$

For the contribution from the diagram in Fig. 7, the only change from the above calculation involves the phonon propagator, and we obtain

$$I_{\text{out}}^{(1)}[f] = -2 \int_{t_i}^t d\tilde{t} \int \frac{dp'}{2\pi\hbar} D_{p-p'}(t, \tilde{t}) f(p - \frac{1}{2}F(t - \tilde{t}), \tilde{t}) \times \exp \left[-\frac{i(t - \tilde{t})}{\hbar} [\epsilon(p' - \frac{1}{2}F(t - \tilde{t})) - \epsilon(p - \frac{1}{2}F(t - \tilde{t}))] \right]. \quad (3.18)$$

The two equations (3.17) and (3.18) have been indexed “in” and “out,” since they correspond to the scattering in and out terms in the Boltzmann picture.

Utilizing the fact that symmetric diagrams give complex-conjugate contributions, as demonstrated in general in the previous section, we obtain the collision-type integral $I^{(1)}$ for the sum of diagrams in Fig. 5.

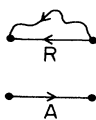


FIG. 6. Lowest-ordered scattering “in” diagram.

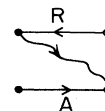


FIG. 7. Lowest-order scattering “out” diagram.

$$\begin{aligned}
 I^{(1)}[f] &= 2 \operatorname{Re}(I_{\text{in}}^{(1)}[f] + I_{\text{out}}^{(1)}[f]) \\
 &= -\frac{1}{\hbar} \int_{t_i}^t d\tilde{t} \int \frac{dp'}{2\pi\hbar} |g_{p'-p}|^2 \{ f(p(t, \tilde{t}), \tilde{t}) [n_{p'-p} \Delta(p', p, t, \tilde{t}) + (1 + n_{-(p'-p)}) \Delta(p, p', t, \tilde{t})] \\
 &\quad - f(p'(t, \tilde{t}), \tilde{t}) [n_{-(p'-p)} \Delta(p, p', t, \tilde{t}) + (1 + n_{p'-p}) \Delta(p', p, t, \tilde{t})] \} , \tag{3.19}
 \end{aligned}$$

where Re implies taking the real part of the subsequent expression, and we have introduced the shorthand

$$\Delta(p, p', t, \tilde{t}) = \frac{2}{\hbar} \cos \left[\frac{1}{\hbar} \int_{\tilde{t}}^t dt' [\epsilon(p'(t, t')) - \epsilon(p(t, t')) + \hbar\omega_{p-p'}] \right] \tag{3.20}$$

and

$$p(t, t') = p - \int_{t'}^t dt'' F . \tag{3.21}$$

We then have the following equation for the Wigner function in the weak-coupling limit:

$$\frac{\partial f}{\partial t} + F \frac{\partial f}{\partial p} = I^{(1)}[f] . \tag{3.22}$$

This is the quantum kinetic equation originally obtained by Levinson (1969). In passing we note that we have written Eq. (3.21) in a form such that, had we considered a time-dependent force, $F = F(t)$, we would have obtained the same equation, Eq. (3.21), except for F being time dependent. Had we considered a degenerate Fermi system, the only change from Eq. (3.19) would be the appearance of the characteristic blocking factor $1 - f$, due to the Pauli principle, but now for the accelerated states as described by Eq. (3.21) (Barker, 1973; Lipavsky *et al.*, 1986).

The quantum kinetic equation differs from the corresponding Boltzmann equation as a consequence of the intracollisional field effect, that is, the appearance of the external field on the right-hand side of Eq. (3.22), and the nonlocal temporal form of the functional $I^{(1)}[f]$. In the classical limit, where Planck's constant is assumed to be zero, $\hbar \rightarrow 0$, the function Δ of Eq. (3.21) becomes a delta function, and we recover the corresponding Boltzmann equation for electron-phonon scattering which does not exhibit any intracollisional field effect. That is, the external field enters only through the usual driving term. The classical concept of an instantaneous energy-conserving collision emerges in this way. In the quantum case, the intracollisional field effect effectively broadens the energy-conserving delta function of the classical collision integral to a nonzero width $(\hbar F \Delta p / 2m)^{1/2}$, where Δp is the effective momentum transfer.

Finding a numerical solution for a quantum kinetic equation such as Eq. (3.22) has proven to be a formidable task, and even with additional assumptions no comprehensive understanding has emerged. For a recent description of the status of these efforts we refer the reader to Jauho (1991). An important point to note is that, once the interaction is treated beyond the lowest order, the interaction itself will give rise to a similar but intrinsic broadening, the collisional broadening effect,

which should therefore be treated on an equal footing with the intracollisional field effect. An effort to implement both effects in a numerical simulation is currently underway (Bertoncini *et al.*, 1990).

A different line of numerical work based on the Feynman path-integral formulation of quantum transport (Feynman *et al.*, 1962), as previously investigated by Thornber and Feynman (1970), is also being pursued. Recently Mason and Hess (1989) succeeded in obtaining the exact time evolution of the density matrix in the presence of an external field for the linear-coupling model. Such a result, in view of modern computing capabilities, lends hope for obtaining a numerical solution of the physically relevant Fröhlich model presented here.

Due to the enormous complexity of the quantum transport equations for semiconductors, as exhibited above, uncontrolled approximations used in the past to simplify matters have led to an inconclusive state of affairs. In view of the importance of understanding dissipative properties of semiconductor structures under high-field conditions, much further effort will be invested, and the simplified approach presented here should therefore prove useful.

IV. DENSITY-MATRIX DESCRIPTION OF A PARTICLE IN A RANDOM POTENTIAL

In the preceding sections we assumed that the environment of the particle constituted a heat bath with which the particle could exchange energy. Another important environment for transport in solids is that of impurities where no energy exchange takes place. During the last decade astonishing progress in the understanding of transport in disordered systems has been achieved. We shall in the remaining sections discuss the physics of disordered conductors in the light of the recently obtained insight.

A. Feynman rules for the impurity-averaged density matrix

For the case of an electron moving in a solid and being scattered mainly by static impurities, we have instead of Eq. (2.1) the Hamiltonian

$$\hat{H} = \hat{H}_p + \hat{H}_i, \tag{4.1}$$

where now

$$\hat{H}_i = V(\hat{x}), \tag{4.2}$$

V being the potential due to the presence of impurities, with the environment of impurities assumed to have no internal dynamics.

The density matrix is, as demonstrated in Sec. II, propagated from its value at time t_i ,

$$\rho(x, x', t) = \int d\bar{x} \int d\bar{x}' J(x, x', t; \bar{x}, \bar{x}', t_i) \rho_i(\bar{x}, \bar{x}'), \tag{4.3}$$

by the propagator of the density matrix J ,

$$J(x, x', t; \bar{x}, \bar{x}', t_i) = \langle x | \hat{U}(t, t_i) | \bar{x} \rangle \langle \bar{x}' | \hat{U}^\dagger(t, t_i) | x' \rangle. \tag{4.4}$$

As in Sec. II, we go to the interaction picture with respect to the particle Hamiltonian \hat{H}_p and obtain, quite analogously to Eq. (2.21), the expression for the density matrix,

$$\begin{aligned} \rho(x, x', t) = & \int d\bar{x} \int d\bar{x}' \int dx_1 \int dx_2 \int dx'_1 \int dx'_2 \langle \bar{x}' | \exp \left[-\frac{i}{\hbar} \hat{H}_p t_i \right] | x'_1 \rangle \\ & \times \langle x'_1 | \tilde{T} \exp \left[\frac{i}{\hbar} \int_{t_i}^t d\bar{t} V(\hat{x}_{\bar{t}}) \right] | x'_2 \rangle \langle x'_2 | \exp \left[\frac{i}{\hbar} \hat{H}_p t \right] | x' \rangle \rho_i(\bar{x}, \bar{x}') \\ & \times \langle x | \exp \left[-\frac{i}{\hbar} \hat{H}_p t \right] | x_1 \rangle \langle x_1 | T \exp \left[-\frac{i}{\hbar} \int_{t_i}^t d\bar{t} V(\hat{x}_{\bar{t}}) \right] | x_2 \rangle \\ & \times \langle x_2 | \exp \left[\frac{i}{\hbar} \hat{H}_p t_i \right] | \bar{x} \rangle. \end{aligned} \tag{4.5}$$

We can now expand the time-ordered exponentials and insert complete sets of states as in Sec. II, and we obtain the diagrammatic expansion of the density matrix ρ as depicted in Fig. 8.

The Feynman rule for dealing with the impurity potential is therefore the following: A cross designates the action of the impurity potential,

$$\text{---} \times \text{---} = \frac{1}{\hbar} V(x), \tag{4.6}$$

and we have integration over such a space-time point (x, t) .

Assuming that the sample under consideration is macroscopic,⁶ so that the electron experiences a random potential, we need only discuss the average properties of physical quantities, which can be done in terms of the statistically averaged density matrix. Assuming the impurity potential to be Gaussian distributed with zero mean (a nonzero mean would only lead to an irrelevant shift in energy), we have $\langle \dots \rangle$ now denotes the statistical average with respect to the ensemble of impurity potentials, that is, different samples)

$$\langle V(x_1) \dots V(x_n) \rangle = \sum_{\text{a.p.p.}} \prod_{i,j} \langle V(x_i) V(x_j) \rangle, \tag{4.7}$$

for n even, and zero for n odd. The sum is over all possible ways of picking the pairs (a.p.p.). For example,

$$\begin{aligned} \langle V(x_1) V(x_2) V(x_3) V(x_4) \rangle &= \langle V(x_1) V(x_2) \rangle \langle V(x_3) V(x_4) \rangle \\ &+ \langle V(x_1) V(x_3) \rangle \langle V(x_2) V(x_4) \rangle \\ &+ \langle V(x_1) V(x_4) \rangle \langle V(x_2) V(x_3) \rangle. \end{aligned} \tag{4.8}$$

The physical realization of this statistical average corresponds to a model in which the positions r_i of the impurities in the sample are assumed to be randomly distributed (Kohn and Luttinger, 1957). In terms of the poten-

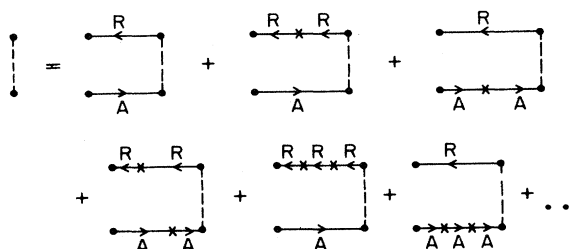


FIG. 8. Diagrammatic representation of the density matrix for a particle in an external potential.

⁶This length scale has been established only recently and is physically the distance L_ϕ over which the electronic wave function maintains phase coherence. Over smaller length scales, the electronic motion is quantum-mechanically coherent. In the subsequent sections a detailed account is given of this new concept in transport theory.

tial V_{imp} of a single impurity at position r_i , we have

$$V(x) = \sum_i V_{\text{imp}}(x - r_i). \quad (4.9)$$

The impurity correlator given by

$$\mathcal{V}(x - x') = \langle V(x)V(x') \rangle \quad (4.10)$$

is related to the potential of the individual impurity by

$$\mathcal{V}(x - x') = n_i \int dr V_{\text{imp}}(x - r)V_{\text{imp}}(x' - r), \quad (4.11)$$

where n_i is the impurity concentration. Furthermore, the above Gaussian description neglects multiple scattering off the same impurity, which is appropriate in the Born approximation. Beyond the Born approximation an identical analysis is carried out in terms of the t matrix (Langer, 1960).

The diagrams for the impurity-averaged density matrix

$$f(x, x', t) = \langle \rho(x, x', t) \rangle, \quad (4.12)$$

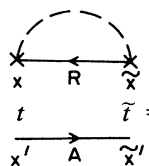
describing the particle motion in the random potential have, according to the above analysis, the form shown in Fig. 9. Performing the impurity average corresponds to pairing the impurity vertices in Fig. 8 in all possible ways. The impurity correlator is represented graphically by a broken line terminated by crosses, and transcribed according to the Feynman rule

$$\begin{array}{c} \times \\ \text{---} \\ \times \end{array} \text{---} \text{---} \text{---} \begin{array}{c} \times \\ \text{---} \\ \times \end{array} = \frac{1}{\hbar^2} \mathcal{V}(x - x'). \quad (4.13)$$

An important point that will enable us to obtain a physical picture from the diagrammatic representation, and that explains the two crosses at the end of the impurity correlator, is that, for an impurity potential with range smaller than the inter-impurity separation, the impurity correlator corresponds to scattering off the same impurity.

B. Quantum kinetic equation for weak impurity scattering

Let us perform an analysis of quantum dynamics in a random potential similar to the one we performed for the interaction with the heat bath, and obtain the temporal



$$\begin{array}{c} \times \\ \text{---} \\ \times \end{array} \text{---} \text{---} \text{---} \begin{array}{c} \times \\ \text{---} \\ \times \end{array} = \frac{1}{\hbar^2} \mathcal{V}(x - \bar{x}) G^R(x, t; \bar{x}, \bar{t}) G^A(\bar{x}', \bar{t}; x', t). \quad (4.16)$$

We can now perform the Fourier transformation as we did in the case of coupling to the heat bath and obtain the equation of motion for the impurity-averaged density matrix in the Wigner representation in a lowest-order treatment of the coupling to the random potential

$$\frac{\partial f}{\partial t} + F \frac{\partial f}{\partial p} = I_1[f], \quad (4.17)$$

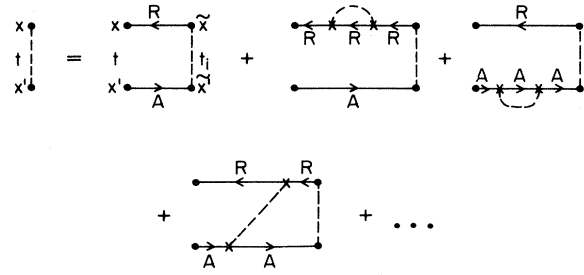


FIG. 9. Diagrammatic representation (lowest order) of the impurity-averaged density matrix.

evolution of the impurity-averaged density matrix in the presence of an external force. We consider the weak-coupling limit and treat the interaction with the impurities perturbatively and to lowest order. In the next section on disordered conductors we shall discuss in detail the validity of such a treatment and its physical significance. To obtain the quantum kinetic equation, treating the interaction with the random potential to lowest order, we expand the exponentials in Eq. (4.5) to second order in the impurity potential, perform the impurity average, and take the time derivative. The equation of motion for the impurity-averaged density matrix then becomes

$$\frac{\partial f(x, x', t)}{\partial t} + \frac{i}{\hbar} \langle x | [\hat{H}_p, \hat{f}(t)] | x' \rangle = -i \tilde{F}_1[f], \quad (4.14)$$

where we have for the functional in the spatial representation

$$\tilde{F}_1[f] = \int d\bar{x}' \int d\bar{x} \int_{t_i}^t d\bar{t} \tilde{J}_1(x, x', t; \bar{x}, \bar{x}', \bar{t}) f(\bar{x}, \bar{x}', \bar{t}), \quad (4.15)$$

and \tilde{J}_1 , the lowest-order irreducible propagator for the impurity-averaged density matrix, has the diagrammatic representation shown in Fig. 10.

As an example of using the Feynman rules, the contribution to \tilde{J}_1 from the first diagram in Fig. 10 is given by

where the functional I_1 in the Wigner representation has the form

$$I_1[f] = -\frac{2}{\hbar^2} n_i \int_{t_i}^t d\tilde{t} \int \frac{dp'}{2\pi\hbar} |V_{\text{imp}}(p-p')|^2 \cos \left[\frac{(t-\tilde{t})}{\hbar} \left[\epsilon(p' - \frac{1}{2}F(t-\tilde{t})) - \epsilon(p - \frac{1}{2}F(t-\tilde{t})) \right] \right] \times [f(p-F(t-\tilde{t}), \tilde{t}) - f(p'-F(t-\tilde{t}), \tilde{t})], \tag{4.18}$$

and $V_{\text{imp}}(p)$ is the Fourier transform of $V_{\text{imp}}(x)$.

The quantum kinetic equation (4.17), which includes the intracollisional field effect for scattering in a weak random potential, has to our knowledge not been considered before, and we shall therefore discuss the assumptions made in arriving at Eq. (4.17), thereby establishing its region of validity. We have assumed that a lowest-order treatment of the random potential is sufficient, that is, higher-order quantum interference effects (to be discussed in detail in the next section), which would result in localization effects, are rendered ineffective by assuming that the length of the sample L is smaller than the localization length ξ , implying that the de Broglie wavelength of the electron is smaller than the impurity mean free path. On the other hand the necessary assumption for the statistical averaging to be meaningful requires the sample dimension to be larger than the phase coherence length L_ϕ (an account of this concept and its role in diffusive electronic transport will be given in the section on weak localization). The phase coherence length in turn must be larger than the impurity mean free path, since inelastic scattering is absent in Eq. (4.17). The phase coherence length is determined by the inelastic collisions (electron-electron or electron-phonon scattering) and thus dependent on the temperature. The application of Eq. (4.17) thus assumes that the impurities, rather than inelastic scattering, give rise to the dominant scattering, but quantum interference effects due to impurity scattering can be neglected. The collisionlike integral, Eq. (4.18), is considerably simpler than in the electron-phonon case, Eq. (3.19), since it corresponds to setting all the phonon frequencies equal to zero (elastic scattering) and the Bose function equal to zero (zero temperature).

In the derivation of Eq. (4.18), we assumed a spatially homogeneous state and did not need to invoke any spatial properties of, say, the irreducible propagator \tilde{J}_1 . To discuss spatially nonhomogeneous states, or to assess the field range of the external force, we need to introduce the skeleton representation of \tilde{J}_1 depicted in Fig. 11, where the upper (retarded) Green's function is given by the set of diagrams depicted in Fig. 12, and similarly for the ad-

vanced Green's function. The resulting change, which is discussed in detail in the next section, consists in the substitution

$$G^R(x, t; x', t') \rightarrow G^R(x, t; x', t') \exp \left[-\frac{|x-x'|}{2l} \right], \tag{4.19}$$

where l is the impurity mean free path. The substitution, Eq. (4.19), corresponds to inclusion of the collisional broadening effect due to impurity scattering. The approximation to the impurity-averaged Green's function constituted by the partial summation of diagrams in Fig. 12 is sufficient if the de Broglie wavelength is smaller than the impurity mean free path, $pl > \hbar$, where p is the momentum of the particle. This is a condition well satisfied for electrons in disordered conductors. The neglected diagrams will involve impurity correlators that cross and, simply due to phase-space restriction for such processes, they are suppressed by the factor \hbar/pl . Obtaining an equation local in the spatial coordinate can now be justified for a spatially nonhomogeneous state if the spatial scale of \tilde{J}_1 , namely l , is smaller than the spatial scale of f , which is set by the spatial variation of the external field, λ_{ext} . Thus we require $l < \lambda_{\text{ext}}$. In this case, we can substitute R for \tilde{R} in f and then perform the \tilde{R} integration as before.

The quantum kinetic equation (4.17) determines the temporal evolution of the Wigner function when the effect of the impurity scattering is weak while the external field can be arbitrarily strong. The quantum nature of the evolution is reflected in the nonlocal temporal form of the influence of the environment, and Eq. (4.17) describes ballistic transport in a field of arbitrary strength. In the classical limit where Planck's constant is assumed to be zero, $\hbar \rightarrow 0$, the rapidly oscillating cosine function in Eq. (4.18) becomes an energy-conserving delta function, and we recover the corresponding Boltzmann equation for hard-sphere scattering, which does not exhibit any intracollisional field effect.

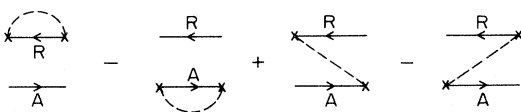


FIG. 10. Diagrammatic representation of the irreducible propagator \tilde{J}_1 .

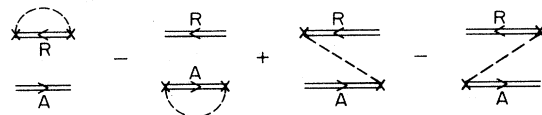


FIG. 11. Skeleton diagram representation for the impurity-averaged irreducible propagator \tilde{J} .

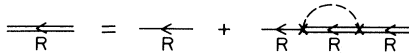


FIG. 12. The upper (retarded) impurity-averaged Green's function.

V. LINEAR RESPONSE OF DISORDERED CONDUCTORS

In the preceding sections we have shown how to derive kinetic equations using a diagrammatic method for the density matrix. The kinetic-equation approach to transport theory is a general method, since it allows, in principle, all nonlinear effects to be considered, whether they be classical or quantum in nature. However, in many practical situations of interest one is interested only in the linear response of the system to the external force, and in the following we shall discuss the linear response of disordered conductors. In the linear-response regime it is possible to obtain diagrammatic representations directly of the physical quantities of interest, such as conductivities and susceptibilities in general. A general feature of the kinetic-equation approach, as compared to the linear-response approach, is that in the former one needs to consider far fewer diagrams. This apparent simplification can in actual calculations, however, soon be overshadowed by complications due to the fact that in the kinetic approach the diagrams represent nonequilibrium quantities.

The linear-response limit is a tremendous simplification in comparison with general nonequilibrium conditions, since linear-response properties are uniquely determined by the equilibrium properties of the system, as expressed through the fluctuation-dissipation theorem (Calen and Welton, 1951). Linear-response theory is of course a well-known textbook subject (Kubo *et al.*, 1983); however, in the standard presentations homogeneity is assumed, an assumption appropriate for discussing the response properties of macroscopic bodies. In the following we shall discuss mesoscopic phenomena for which such an assumption is invalid, and we shall therefore present the general formulation of linear-response theory. In contrast to the standard treatments (Lax, 1958), we shall base our presentation on the diagram technique developed above for the density matrix and thereby benefit from the simple physical picture of single-particle transport.

In this section, we shall therefore apply the diagrammatic technique for the density matrix to a discussion of linear response. We shall specifically discuss electrical conductivity, and in particular discuss quantum effects due to impurity scattering. For completeness, in the following we shall represent the external electric field **E** by a vector potential **A** (we shall in this section use an explicit many-dimensional notation),

$$\mathbf{E} = - \frac{\partial \mathbf{A}}{\partial t} , \tag{5.1}$$

and not, as in Sec. II, by a scalar potential. The two representations can be handled with an equal amount of labor, as they are equivalent by gauge invariance.

A. The conductivity tensor

In this section we derive the general expression for the conductivity tensor for a noninteracting electron gas in an impurity field. We start by considering a single particle and show that, since the scattering is elastic, we can easily incorporate the fermionic character of the electrons.

We wish to calculate the current response to lowest order in the electric field. The system we shall have in mind is that of a particle interacting with impurities through an impurity potential *V*. The Hamiltonian in question is therefore

$$\hat{H} = \frac{\hat{\mathbf{P}}_{\text{kin}}^2}{2m} + V(\hat{\mathbf{x}}) = \hat{H}_0 + \hat{H}_{A(t)} , \tag{5.2}$$

where

$$\hat{H}_0 = \frac{\hat{\mathbf{P}}_{\text{can}}^2}{2m} + V(\hat{\mathbf{x}}) \tag{5.3}$$

is the Hamiltonian for the particle in the impurity field, and the interaction of the particle and the classical field is given by

$$\begin{aligned} \hat{H}_{A(t)} &= \int d\mathbf{x} \hat{\mathbf{j}}(\mathbf{x}) \cdot \mathbf{A}(\mathbf{x}, t) \\ &= \frac{e}{2m} [\hat{\mathbf{P}}_{\text{can}} \cdot \mathbf{A}(\hat{\mathbf{x}}, t) + \mathbf{A}(\hat{\mathbf{x}}, t) \cdot \hat{\mathbf{P}}_{\text{can}}] \\ &\quad + \frac{e^2}{2m} \mathbf{A}^2(\hat{\mathbf{x}}, t) . \end{aligned} \tag{5.4}$$

In the presence of a vector potential, the current-density operator is ($\{ , \}$ denotes the anticommutator)

$$\hat{\mathbf{J}}(\mathbf{x}) = \frac{e}{2m} \{ \hat{\mathbf{P}}_{\text{kin}}, \hat{n}(\mathbf{x}) \} , \tag{5.5}$$

where $\hat{n}(\mathbf{x})$ is the density operator,

$$\hat{n}(\mathbf{x}) = \delta(\mathbf{x} - \hat{\mathbf{x}}) , \tag{5.6}$$

and the kinematical momentum operator is related to the canonical momentum operator through the minimal coupling relation

$$\hat{\mathbf{P}}_{\text{kin}} = \hat{\mathbf{P}}_{\text{can}} - e \mathbf{A}(\hat{\mathbf{x}}, t) . \tag{5.7}$$

For the current density at time *t* in a quantum-statistical ensemble characterized by the statistical operator $\hat{\rho}(t)$, we have

$$\begin{aligned}
 \mathbf{j}(\mathbf{x}, t) &= \text{Tr}[\hat{\rho}(t)\hat{\mathbf{j}}(\mathbf{x})] \\
 &= \frac{e\hbar}{2im} \left[\frac{\partial}{\partial \mathbf{x}} - \frac{\partial}{\partial \mathbf{x}'} \right] \rho(\mathbf{x}, \mathbf{x}', t) \Big|_{\mathbf{x}'=\mathbf{x}} - \frac{e^2}{m} \mathbf{A}(\mathbf{x}, t)\rho(\mathbf{x}, \mathbf{x}, t).
 \end{aligned} \tag{5.8}$$

Since the second, diamagnetic, term in Eq. (5.8) is explicitly linear in the external field, we can to linear order replace $\rho(t)$ by $\rho_0(t)$, the statistical operator evolved by the unperturbed Hamiltonian \hat{H}_0 .

To calculate the density matrix to linear order in the external electric field, we write the evolution operator \hat{U} in the interaction picture with respect to the unperturbed Hamiltonian \hat{H}_0

$$\begin{aligned}
 \hat{U}(t, t') &= \exp \left[-\frac{i}{\hbar} \hat{H}_0 t \right] T \exp \left[-\frac{i}{\hbar} \int_{t'}^t d\bar{t} \hat{H}_A(\bar{t}) \right] \\
 &\quad \times \exp \left[\frac{i}{\hbar} \hat{H}_0 t' \right],
 \end{aligned} \tag{5.9}$$

where

$$\hat{H}_A(t) = \exp \left[-\frac{i}{\hbar} \hat{H}_0 t \right] \hat{H}_{A(t)} \exp \left[\frac{i}{\hbar} \hat{H}_0 t \right] \tag{5.10}$$

is the perturbation in the interaction picture. In the linear-response regime, we can in the perturbation $\hat{H}_{A(t)}$ omit the quadratic term in the external field.

If we now expand the density-matrix propagator to lowest order in the field, for the linear corrections to the density matrix ρ we obtain the expression given by the first two diagrams of Fig. 13. In linear response, we can let the initial density matrix be evolved in time by \hat{H}_0 up until the time of interaction with the external field, to obtain the second set of diagrams of Fig. 13. The current vertex couples the particle current density to the vector potential at the space-time point in question according to the Feynman rule

$$\begin{aligned}
 \text{---} \text{---} \text{---} &= \frac{e}{2im} \left[\overleftarrow{\frac{\partial}{\partial \mathbf{x}}} \cdot \mathbf{A}(\mathbf{x}, t) - \mathbf{A}(\mathbf{x}, t) \cdot \frac{\partial}{\partial \mathbf{x}} \right],
 \end{aligned} \tag{5.11}$$

where the upper arrow on $\overleftarrow{\partial}/\partial \mathbf{x}$ is meant to designate that the differential operator operates on the Green's function to the left.

The linear correction to the density matrix is therefore, according to the application of the Feynman rules to the diagrams of Fig. 13, given by the expression

$$\begin{aligned}
 \rho^{(1)}(\mathbf{x}, \mathbf{x}', t) &= \frac{e}{2im} \int d\mathbf{x}_1 \int d\mathbf{x}'_1 \int_{t_i}^t dt_1 \left[G^R(\mathbf{x}, t; \mathbf{x}_1, t_1) \left\{ \overleftarrow{\frac{\partial}{\partial \mathbf{x}_1}} \cdot \mathbf{A}(\mathbf{x}_1, t_1) - \mathbf{A}(\mathbf{x}_1, t_1) \cdot \frac{\partial}{\partial \mathbf{x}_1} \right\} \rho_0(\mathbf{x}_1, \mathbf{x}'_1, t_1) G^A(\mathbf{x}'_1, t_1; \mathbf{x}', t) \right. \\
 &\quad \left. + G^R(\mathbf{x}, t; \mathbf{x}_1, t_1) G^A(\mathbf{x}'_1, t_1; \mathbf{x}', t) \left\{ \overleftarrow{\frac{\partial}{\partial \mathbf{x}'_1}} \cdot \mathbf{A}(\mathbf{x}'_1, t_1) - \mathbf{A}(\mathbf{x}'_1, t_1) \cdot \frac{\partial}{\partial \mathbf{x}'_1} \right\} \right. \\
 &\quad \left. \times \rho_0(\mathbf{x}_1, \mathbf{x}'_1, t_1) \right].
 \end{aligned} \tag{5.12}$$

Let us assume that prior to the time the field is switched on, the particle has been in contact with a heat bath, so that its statistical operator is the thermal one,

$$\hat{\rho}_i = \sum_{\lambda} f_{\lambda} |\lambda\rangle \langle \lambda|, \tag{5.13}$$

where the $|\lambda\rangle$'s are the exact impurity eigenstates of \hat{H}_0 ,

$$\hat{H}_0 |\lambda\rangle = \epsilon_{\lambda} |\lambda\rangle. \tag{5.14}$$

At this point we could continue the discussion of a single particle, which in many cases would be appropriate, for example, for electron dynamics in semiconductors. Since we wish to be able to consider the dynamics of an electron gas, we must bear in mind that in quantum mechanics identical particles are indistinguishable, which has

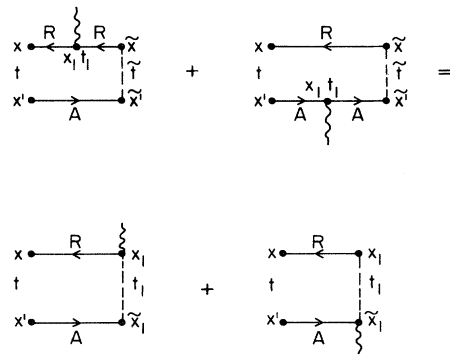


FIG. 13. Linear-response diagrams for the density matrix.

consequences even for noninteracting particles. In the linear-response regime we can take advantage of the fact that for noninteracting electrons the fermionic feature can be incorporated immediately. Instead of continuing discussing a single particle in the impurity potential, we therefore let $\hat{\rho}_i$ denote the statistical operator describing a noninteracting electron gas, at temperature T and with density n , in the impurity potential by choosing the probabilities f_λ in accordance with the Pauli principle so that

$$f_\lambda = \frac{1}{\exp[(\epsilon_\lambda - \epsilon_F)/k_B T] + 1}, \quad (5.15)$$

where ϵ_F is the Fermi energy of the electron gas.

The descriptions of a single particle and of a noninteracting electron gas in an impurity field are equivalent because the scattering is independent of the electron distribution, thereby rendering the Pauli exclusion principle inoperative on the dynamics. We could also explicitly introduce the spin degree of freedom of the electron. However, since the spin in the following plays no dynamic role, but would only amount to multiplying in equations, such as the right-hand side of Eq. (5.21), by a factor of 2, we shall neglect the spin in the following. We note, however, that this choice is made for simplicity in presenting the fundamental features of quantum transport in disordered conductors and represents no limitation in principle. We could straightforwardly introduce the spin degree of freedom of the electron and thereby discuss scattering off magnetic impurities and the effects of spin-orbit scattering.

In linear response, each monochromatic contributes additively, so without loss of generality we can concentrate on a specific frequency ω of the electric field

$$\mathbf{E}(\mathbf{x}, t) = \mathbf{E}_\omega(\mathbf{x}) e^{-i\omega t}, \quad (5.16)$$

so that the vector potential is given by

$$\mathbf{A}(\mathbf{x}, t) = \mathbf{A}_\omega(\mathbf{x}) e^{-i\omega t}, \quad (5.17)$$

with the Fourier component

$$\mathbf{A}_\omega(\mathbf{x}) = \frac{1}{i\omega} \mathbf{E}_\omega(\mathbf{x}). \quad (5.18)$$

Since we are interested in the steady state, we can let the initial time t_i in which the external field is switched on be in the remote past so that t_i approaches minus infinity. The final ingredient we need in order to extract the temporal Fourier component at frequency ω of the current density, Eq. (5.8), is to make use of the fact that the retarded and advanced Green's functions have the spectral representation in terms of the complete set of eigenstates of the Hamiltonian, \hat{H}_0 , for the particle in the impurity field

$$G^{R(A)}(\mathbf{x}, \mathbf{x}'; \epsilon) = \hbar \sum_\lambda \frac{\psi_\lambda^*(\mathbf{x}') \psi_\lambda(\mathbf{x})}{\epsilon - \epsilon_{\lambda(\pm)} \pm i0^+}, \quad (5.19)$$

where $G^{R(A)}(\mathbf{x}, \mathbf{x}'; \epsilon)$ is the temporal Fourier transform of $G^{R(A)}(\mathbf{x}, t; \mathbf{x}', t')$, and $\psi_\lambda(x) = \langle x | \lambda \rangle$ is the exact impurity eigenstate corresponding to the energy eigenvalue ϵ_λ . Equation (5.19) is readily obtained from the definition (2.29) by inserting complete sets of energy eigenstates. Upon inserting into Eq. (5.12), and subsequently using Eq. (5.8), we then obtain for the frequency-dependent current response

$$\mathbf{j}_\alpha(\mathbf{x}, \omega) = \int d\mathbf{x}' \sigma_{\alpha\beta}(\mathbf{x}, \mathbf{x}', \omega) [\mathbf{E}_\omega(\mathbf{x}')]_\beta, \quad (5.20)$$

where the conductivity tensor is

$$\begin{aligned} \sigma_{\alpha\beta}(\mathbf{x}, \mathbf{x}', \omega) = & -\frac{1}{4\pi} \left[\frac{e}{m} \right]^2 \int_{-\infty}^{\infty} d\epsilon \frac{f(\epsilon) - f(\epsilon + \hbar\omega)}{\omega} [G^R(\mathbf{x}, \mathbf{x}'; \epsilon + \hbar\omega) - G^A(\mathbf{x}, \mathbf{x}'; \epsilon + \hbar\omega)] \\ & \times (\vec{\nabla}_{\mathbf{x}})_\alpha (\vec{\nabla}_{\mathbf{x}'})_\beta [G^R(\mathbf{x}', \mathbf{x}; \epsilon) - G^A(\mathbf{x}', \mathbf{x}; \epsilon)], \end{aligned} \quad (5.21)$$

and where we have introduced the abbreviated notation

$$\vec{\nabla}_{\mathbf{x}} = \frac{1}{2} \left[\frac{\partial}{\partial \mathbf{x}} - \frac{\tilde{\partial}}{\partial \mathbf{x}} \right]. \quad (5.22)$$

In the course of the derivation of Eq. (5.21), the diamagnetic current has cancelled the off-shell part in the first term on the right-hand side of Eq. (5.8), so that only the thermal layer near the Fermi surface contributes to the conductivity, as expected.

The current density Eq. (5.20), is expressed in terms of the exact solution of the Schrödinger equation or equivalently the Liouville-von Neumann equation. The conductivity tensor, Eq. (5.21), contains all information specific to the sample, such as impurity configuration,

geometry, and connection to leads. The linear-response relation, Eq. (5.20), therefore does not immediately describe the dissipative experimental linear relationship between macroscopic currents and voltages. In order to do this we must explicitly deal with the interactions of the system under investigation, the coupling of the sample to the environment, and the fact that electrons are entering and leaving the sample. In the present case this is not a delicate matter and can be done by simply imposing boundary conditions, and as we show in Sec. V.D we are led to a description equivalent to the Landauer approach for mesoscopic samples, in which phase-randomizing electron reservoirs, sources and sinks for electrons, provide the necessary means for destroying coherence, that is, the dissipation necessary for establishing the steady

state of linear response. In the case of macroscopic samples we expect such an issue as the presence of leads to be irrelevant, as we indeed subsequently demonstrate. However, what is nontrivial is the length scale defining the macroscopic scale, the quantitative understanding of which constitutes a major recent advance in the description of disordered conductors. In the following sections we shall discuss the conductance of macroscopic samples with particular emphasis on quantum-mechanical effects, and subsequently the sample-specific properties due to quantum effects in mesoscopic samples.

B. The classical conductance

As mentioned above, we are here interested only in macroscopic samples. The properties of a macroscopic sample can be ascertained through a few macroscopic parameters. In the present case of electrons scattered by impurities, the mean concentration of the impurities (assumed to be constant on the average) or, equivalently, the elastic mean free path l characterizes the conduction properties. A macroscopic sample is therefore characterized by its average conductance (inverse resistance) tensor

$$\langle G_{\alpha\beta}^{(\omega)} \rangle = L^{-2} \int d\mathbf{x} \int d\mathbf{x}' \langle \sigma_{\alpha\beta}(\mathbf{x}, \mathbf{x}', \omega) \rangle, \quad (5.23)$$

where $\langle \sigma_{\alpha\beta}(\mathbf{x}, \mathbf{x}', \omega) \rangle$ is the impurity average of the conductivity tensor, Eq. (5.21), and L is the length of the sample. We shall show that the macroscopic length scale is determined by quantum-mechanical effects, thereby introducing a new concept in transport theory, the phase coherence length L_ϕ .

The impurity-averaged conductivity tensor is described by diagrams like those in Fig. 14, as can be seen from the following consideration. The typical structure of the impurity-averaged conductivity diagram is the impurity average of a product of Green's functions, for example,

$$\sigma^{RA} = \langle G^R(\mathbf{x}, \mathbf{x}'; \epsilon + \hbar\omega) G^A(\mathbf{x}', \mathbf{x}; \epsilon) \rangle, \quad (5.24)$$

where the Green's functions contain complete information on the electronic motion in the impurity potential. This impurity average is analogous to the one we performed in Sec. IV for the density matrix: Expand G^R and G^A , according to Eq. (2.29), in terms of the impurity potential as in Fig. 8, and perform the pairwise connections as in Fig. 9. As in Figs. 9, 10, and 11, there are two distinct classes of diagrams: a class in which the retarded Green's function G^R and the advanced Green's function G^A are not connected by impurity correlators, and a class in which they are connected, as depicted in Fig. 14.

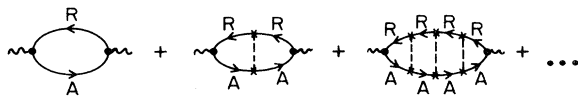


FIG. 14. The classical conductance diagrams.

In these and subsequent diagrams we have, for visual clarity, depicted the impurity-averaged Green's functions by a single line and not as a double-line object as in Fig. 12. The contribution to the impurity-averaged conductivity tensor of a given diagram is therefore calculated by the same Feynman rules as stated for the density matrix.

For purposes of this discussion, we shall assume that the electron gas is degenerate, that is, all other energies are small compared to the Fermi energy ϵ_F . Since the scattering is elastic this is no restriction; had we preferred to discuss the mobility of a single particle we could equally well have concentrated on any other energy. The energy integration in Eq. (5.21) can then be performed, since for frequencies and temperatures that are small compared to the scale set by the Fermi energy, $\hbar\omega, k_B T < \epsilon_F$, we can exploit the degeneracy of the electron gas to substitute for the temperature-dependent term the delta function

$$\frac{f(\epsilon) - f(\epsilon + \hbar\omega)}{\hbar\omega} \approx \delta(\epsilon - \epsilon_F). \quad (5.25)$$

Therefore only electrons on the Fermi surface contribute to the conductivity, as expected according to the Pauli principle.

Here we digress briefly to obtain the expression for the impurity-averaged Green's function, Eq. (4.19). Without loss of generality for our discussion, we can assume a delta-function correlator for the impurity correlator, Eq. (4.10),

$$\mathcal{V}(\mathbf{x} - \mathbf{x}') = u^2 \delta(\mathbf{x} - \mathbf{x}'), \quad (5.26)$$

which according to Eq. (4.11) corresponds to the limit of dense point scatterers.

As noted earlier, the impurity-averaged Green's function is determined by the set of diagrams depicted in Fig. 12, provided that the electronic (Fermi) wavelength is small compared to the impurity mean free path or, equivalently, the energy uncertainty is small, $\epsilon \tau_\epsilon > \hbar$, where the impurity mean free time τ_ϵ is related to the impurity correlator strength by

$$\frac{\hbar}{\tau_\epsilon} = 2\pi N(\epsilon) u^2, \quad (5.27)$$

where $N(\epsilon)$ is the density of states (per spin) of the electrons. This result is readily obtained by Fourier transforming the analytical expression in the spatial representation corresponding to Fig. 12. For the retarded impurity-averaged Green's function we then obtain

$$\langle G^R(\epsilon, \mathbf{p}) \rangle = \frac{\hbar}{\epsilon - \epsilon_p - \Sigma^R(\epsilon, \mathbf{p})}, \quad (5.28)$$

where the retarded self-energy, that is, the insertion in the rightmost diagram of Fig. 12, is given by

$$\Sigma^R(\epsilon, \mathbf{p}) = \frac{u^2}{\hbar} \int \frac{d\mathbf{p}'}{(2\pi\hbar)^d} \langle G^R(\epsilon, \mathbf{p}') \rangle. \quad (5.29)$$

Substituting the free-particle propagator [obtained from

Eq. (3.15) by setting the external force equal to zero, $F=0$]

$$G_0^R(\epsilon, \mathbf{p}) = \frac{\hbar}{\epsilon - \epsilon_p + i0}, \quad (5.30)$$

into Eq. (5.29), we obtain

$$\Sigma^R(\epsilon, \mathbf{p}) = -i \frac{\hbar}{2\tau_\epsilon} + c(\epsilon). \quad (5.31)$$

The real part of the self-energy, $c(\epsilon)$, is, in the present free-electron model with short-range impurities, in fact infinite. The contribution from large momenta are in reality cut off, since contributions from processes with large momenta are small. A finite range of the impurity potential will then transform $c(\epsilon)$ into a slowly varying function of energy ϵ , which only results in an irrelevant shift in the chemical potential ϵ_F . The effect of the random potential is therefore to shift the pole of the Green's function off the real axis, thereby giving momentum eigenstates a finite lifetime τ . The slow energy dependence of the lifetime, or equivalently the density of states, can be neglected when considering the electric current, in contrast to the case of the thermoelectric current. The particular energy picked here is the Fermi energy, or if we consider only one particle, its energy, and we shall henceforth at times drop the energy subscript. Since the other relevant quantities, density of states and range of impurity potential, involved in the calculation of the self-energy vary only on the scale of the Fermi energy, the result for the imaginary part of the self-energy in Eq. (5.31) is not dependent on the substitution in Eq. (5.29) of the free propagator for the full propagator provided $\epsilon_F \tau > \hbar$, and we therefore have for the impurity-averaged retarded Green's function

$$\langle G^R(\epsilon, \mathbf{p}) \rangle = \frac{\hbar}{\epsilon - \epsilon_p + i\hbar/2\tau} = G_\epsilon^R(\mathbf{p}), \quad (5.32)$$

where the shorthand notation has been introduced in order to avoid brackets. Equation (5.32) for the impurity-averaged Green's function corresponds by simply Fourier transforming to an exponential decay of momentum correlations with the rate $1/\tau$ as in the classical Drude theory (Ashcroft and Mermin, 1976).

By Fourier transforming Eq. (5.32) and calculating the integral by the residue method, we obtain the spatial representation

$$\begin{aligned} \langle G^R(\mathbf{x}, \mathbf{x}', \epsilon) \rangle &= -\frac{m}{2\pi\hbar} \frac{\exp\{i|\mathbf{x}-\mathbf{x}'|(ik_\epsilon - 1/2l_\epsilon)\}}{|\mathbf{x}-\mathbf{x}'|} \\ &= G_\epsilon^R(\mathbf{x}, \mathbf{x}'), \end{aligned} \quad (5.33)$$

where $k_\epsilon = (1/\hbar)\sqrt{2m\epsilon}$ is the electronic wave vector, and $l_\epsilon = (\hbar/m)k_\epsilon\tau_\epsilon$ the impurity mean free path. Equation (5.33) applies to the case in which the sample dimensions are larger than the impurity mean free path, so that the motion in the impurity field is three dimensional. In the strictly two-dimensional case, which can be realized for instance in MOSFET's, one should use the corre-

sponding two-dimensional expression. The impurity-averaged Green's function, Eq. (5.33), is translationally and rotationally invariant, as the average over all impurity configurations leaves no preferred direction.

Neglecting, for the moment, diagrams in which the impurity correlator connects the retarded and advanced Green's functions, we obtain by inserting Eq. (5.33) into Eq. (5.23) for the conductance, and using the property

$$G_\epsilon^A(\mathbf{x}, \mathbf{x}') = [G_\epsilon^R(\mathbf{x}', \mathbf{x})]^*, \quad (5.34)$$

the well-known Drude expression for the macroscopic conductance

$$\langle G_{\alpha\beta}^{(\omega)} \rangle = \frac{ne^2\tau}{m(1-i\omega\tau)} L^{d-2} \delta_{\alpha\beta}, \quad (5.35)$$

where d is the dimension of the sample.

The diagrams depicted in Fig. 14 are all formally of the same order of magnitude, since an impurity correlator with its two accompanying Green's functions is of order unity and must be treated on an equal footing. Inclusion of the diagrams in Fig. 14, where the retarded and advanced particle line is connected, leads again to the conductance formula, Eq. (5.35), except that the impurity mean free time τ is now replaced by the transport time for a general impurity potential (Edwards, 1958; Langer, 1960), expressing the simple fact that forward scattering is not effective in degrading the current. In the present delta-function correlator model, Eq. (5.26), these times are identical, as each scattering direction is weighted equally.

The typical term in the conductivity tensor, Eq. (5.21), is according to Eq. (5.24) seen to be basically the probability for the particle to move between different points in the sample. In obtaining the classical result for the macroscopic conductance we have assumed that the quantum interference terms are averaged to zero when the impurity average is performed. This corresponds to neglecting the wave nature of electronic motion and is therefore only correct to lowest order in the electronic wavelength over the impurity mean free path. In the following section we shall see that a certain class of self-intersecting classical paths are resilient to the impurity average, giving rise to the phenomenon of localization in random media.

C. Weak localization

The theory of weak localization dates back to the seminal work of Abrahams *et al.* (1979) on the scaling theory of conductance and developed rapidly to a comprehensive understanding of the quantum corrections to classical conductivity (Al'tshuler, Aronov, Khmel'nitskii, and Larkin, 1982). The weak-localization effect was soon realized to be the result of a simple type of quantum-mechanical interference (Larkin and Khmel'nitskii, 1982; Khmel'nitskii, 1984), and the resulting physical insight eventually led to a quantitative understanding of mesoscopic phenomena in disordered conductors. Below we

use the diagrammatic technique to examine weak-localization phenomena, paying particular attention to the quantum-mechanical interference.

In the preceding section we derived the expression for the classical conductance as the limiting case in which the quantum-mechanical wave nature of electronic motion is neglected. The type of diagram we have so far neglected is that in which impurity correlators cross. As noted earlier, such contributions are smaller by a factor $\hbar/\epsilon_F\tau$ and thus constitute the quantum corrections to the classical conductance. All the diagrams in Fig. 15 are formally of the same order of magnitude and must be summed. In the time-reversal-invariant situation, the maximally crossed diagrams in Fig. 15 in fact exhibit singular behavior, and we shall therefore consider the explicitly time-dependent situation in which the external frequency ω is not equal to zero. We note that, for conductance diagrams where impurity correlators connect the upper and lower particle lines, we need only consider those in which retarded and advanced are connected; the other combinations exhibit no singular behavior, as the impurity scattering effectively separates the momentum integrations. The maximally crossed diagrams were originally studied by Langer and Neal (1966); however, their physical significance was not realized, and consequently a wrong regularization of their singular behavior was employed. As previously, the free-electron model with isotropic scattering will be used for convenience; band structure and anisotropy can be handled with equal ease, (Rainer and Bergmann, 1985).

The impurity-averaged Green's function, Eq. (5.33), decays exponentially with a spatial range equal to the mean free path $l=v_F\tau$, where v_F is the Fermi velocity. As will become clear, the spatial scale of variation of the so-called Cooperon, the sum of the maximally crossed diagrams of Fig. 15, is quite different and typically much larger; this is the phase coherence length. In the diagrams of Fig. 15, the impurity-averaged Green's functions attached to the sum of the maximally crossed diagrams, $C_\omega(\mathbf{x}, \mathbf{x}')$, therefore require the starting and end points of the Cooperon to be within a mean free path, which on the scale of variation of the Cooperon amounts to setting its spatial arguments equal. The conductivity diagram depicted in Fig. 15 can therefore be evaluated, leading to the quantum correction to the macroscopic conductance

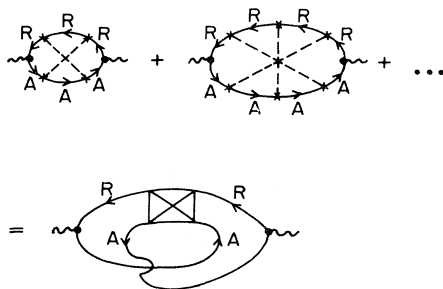


FIG. 15. The quantum correction conductance diagrams.

$$\delta \langle G_{\alpha\beta}^{(\omega)} \rangle = -\frac{e^2 D \tau}{\pi \hbar} L^{-2} \delta_{\alpha\beta} \int d\mathbf{x} C_\omega(\mathbf{x}, \mathbf{x}), \quad (5.36)$$

where $D=v_F l/d$ is the diffusion constant in d dimensions. For samples of size larger than the mean free path, $L > l$, the diffusion process is effectively three dimensional, so that one should use the value $d=3$ in the diffusion constant.

The sum of the maximally crossed diagrams, the Cooperon $C_\omega(\mathbf{x}, \mathbf{x}')$, is generated by the iterative equation depicted in Fig. 16, whose analytical expression, according to the Feynman rules, is given by [with the normalization convention chosen in Eq. (5.36)]

$$C_\omega(\mathbf{x}, \mathbf{x}') = \delta(\mathbf{x} - \mathbf{x}') + \int d\mathbf{x}'' \bar{J}_\omega^c(\mathbf{x}, \mathbf{x}'') C_\omega(\mathbf{x}'', \mathbf{x}'), \quad (5.37)$$

where the insertion \bar{J}_ω^c is given by

$$\bar{J}_\omega^c(\mathbf{x}, \mathbf{x}') = \frac{u^2}{\hbar^2} G_{\epsilon_F + \hbar\omega}^R(\mathbf{x}, \mathbf{x}') G_{\epsilon_F}^A(\mathbf{x}, \mathbf{x}'). \quad (5.38)$$

The slow variation of C_ω on the scale of the mean free path, which is the spatial extent of the function \bar{J}_ω^c as evident from Eq. (5.33), makes a low-order Taylor-expansion in Eq. (5.37) sufficient, so that we obtain on a length scale much larger than the mean free path

$$\left[\left(1 - \int d\mathbf{r} \bar{J}_\omega^c(\mathbf{r}) \right) - \frac{1}{2d} \left[\int d\mathbf{r} \mathbf{r}^2 \bar{J}_\omega^c(\mathbf{r}) \right] \nabla_x^2 \right] C_\omega(\mathbf{x}, \mathbf{x}') = \delta(\mathbf{x} - \mathbf{x}'), \quad (5.39)$$

where $\bar{J}_\omega^c(\mathbf{r})$ equals $\bar{J}_\omega^c(\mathbf{x}, \mathbf{x}')$ for $\mathbf{r} = \mathbf{x} - \mathbf{x}'$.

The integrals needed in Eq. (5.39) can now be performed by substituting Eq. (5.33); assuming $\epsilon_F\tau > \hbar$ and $\hbar\omega < \epsilon_F$, we obtain

$$\int d\mathbf{r} \bar{J}_\omega^c(\mathbf{r}) = \frac{1}{1 - i\omega\tau}, \quad (5.40)$$

$$\frac{1}{2d} \int d\mathbf{r} \mathbf{r}^2 \bar{J}_\omega^c(\mathbf{r}) = \frac{D\tau}{(1 - i\omega\tau)^3}. \quad (5.41)$$

The moments in Eqs. (5.40) and (5.41) have a simple physical interpretation. $\bar{J}_\omega^c(\mathbf{r})$ for ω equal to zero is the

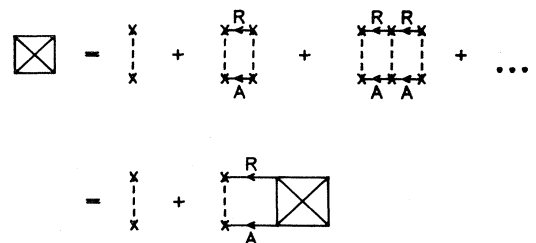


FIG. 16. The iterative equation for the sum of the maximally crossed diagrams.

probability density, on the length scale of the mean free path, for finding the particle at position \mathbf{r} as seen from the definition, Eq. (5.38). The normalization of this probability, that is, particle conservation, is therefore expressed by Eq. (5.40), and Eq. (5.41) is the statement that the motion in the random potential is diffusive. Hence, for small frequencies, $\omega\tau < 1$, and for length scale variations $1/q$ larger than the mean free path, $ql < 1$, we obtain the following equation determining the Cooperon:

$$(-i\omega - D\nabla_{\mathbf{x}}^2)C_{\omega}(\mathbf{x}, \mathbf{x}') = \frac{1}{\tau}\delta(\mathbf{x} - \mathbf{x}') . \quad (5.42)$$

The solution of Eq. (5.42) is immediately obtained by Fourier transformation. Inserting it in Eq. (5.36) for the conductance, we find that in a quasi-two-dimensional system, where the thickness of the film is smaller than $\sqrt{D/\omega}$, the quantum correction to the conductance exhibits the singular behavior (Gor'kov *et al.*, 1979)

$$\delta\langle G_{\alpha\beta}^{(\omega)} \rangle = -\frac{e^2}{4\pi^2\hbar}\delta_{\alpha\beta}\ln\frac{1}{\omega\tau} . \quad (5.43)$$

We note that the quantum correction to the conductance, in the limit of a large two-dimensional sample which we considered here, is finite only because we considered a time-dependent external field. This feature can be understood once the physical origin of the weak-localization effect has been realized. We shall shortly demonstrate that the structure of the diagrams involved lends itself to a simple physical interpretation. Before doing so, we note that the quantum correction to the conductance, Eq. (5.43), compared to the classical contribution, Eq. (5.35), is of relative order $1/k_F l$ (in the considered quasi-two-dimensional case). This is the fraction of a wave with wave vector k_F scattered back to its source by a random medium with mean obstacle separation l , when the wavelength is smaller than the obstacle separation, $k_F l > 1$.

The physical process describing the classical conductance is velocity relaxation or, equivalently, according to the Einstein relation, diffusion. which in our diagrammatic language is described by the diffusion propagator depicted in Fig. 17. Employing the diagrammatic technique for the impurity-averaged density matrix, we see from Fig. 9 that the diffusion propagator is just the

leading-order, in $1/k_F l$, contribution to the impurity-averaged diagonal density matrix when the particle initially, at time t' , is prepared in a state of definite position, say \mathbf{x}' :

$$f_i(\mathbf{x}_1, \mathbf{x}'_1) = \delta(\mathbf{x}_1 - \mathbf{x}')\delta(\mathbf{x}'_1 - \mathbf{x}') . \quad (5.44)$$

That is, the diffusion propagator is the leading-order contribution to the propagator of the impurity-averaged diagonal density matrix, $J^D(\mathbf{x}, \mathbf{x}, t; \mathbf{x}', \mathbf{x}', t')$, and accordingly the classical conditional probability for diffusing between space-time points.

For calculation purposes it is convenient to introduce the ‘‘Diffuson,’’ obtained from the diffusion propagator J^D by deleting the external legs, and denoted by the box in Fig. 17. The Diffuson is determined by a similar iterative equation to that used for the Cooperon, depicted diagrammatically in Fig. 16, with the important difference that one of the particle lines, say the advanced one, is reversed. The Diffuson will therefore be determined by the same equation as the Cooperon, Eq. (5.37), except that \tilde{J}_{ω}^c is now replaced by the diffusion insertion \tilde{J}_{ω}^D given by

$$\tilde{J}_{\omega}^D(\mathbf{x}, \mathbf{x}') = \frac{u^2}{\hbar^2}G_{\epsilon_F + \hbar\omega}^R(\mathbf{x}, \mathbf{x}')G_{\epsilon_F}^A(\mathbf{x}', \mathbf{x}) . \quad (5.45)$$

In a time-reversal-invariant situation the two insertions are equal, $\tilde{J}_{\omega}^c = \tilde{J}_{\omega}^D$, and the Diffuson satisfies the same diffusion equation as the Cooperon, Eq. (5.42). However, the Diffuson and the Cooperon will no longer satisfy the same equations once quantum coherence is disrupted by interaction effects, which must be taken into account when the analysis is not limited to zero temperature, or when the coherence is influenced by an external magnetic field, magnetic impurities, or spin-orbit scattering. The Diffuson, or rather the diffusion propagator, will in all cases describe the conditional probability for diffusion, whereas this is not the case for the Cooperon. In view of the reversal of one of the particle lines, the Cooperon is therefore also referred to as the particle-particle ladder, and the Diffuson as the particle-hole ladder. For the present one-particle situation, however, physical insight may be gained by interpreting the diagrams as products of amplitudes for various alternative classical paths. The diffusion propagator or, equivalently, the Diffuson is, according to the diagrammatic representation seen to describe the ‘‘amplitude for scattering sequence times the complex conjugate of the same amplitude,’’ thus describing a probability, the spreading of the probability density of the diffusing particle. Although the Cooperon in a time-reversal-invariant situation is described by the same diffusion equation, Eq. (5.42), its physical content is quite different. We can see from the diagrammatic representation that the Cooperon describes ‘‘amplitude for scattering sequence times the complex conjugate of the amplitude for the opposite scattering sequence.’’ According to Eq. (5.36) we need only consider scattering sequences that start and end at the same point (on the scale of the mean free path). The quantum correction to the conductance is thus the result of

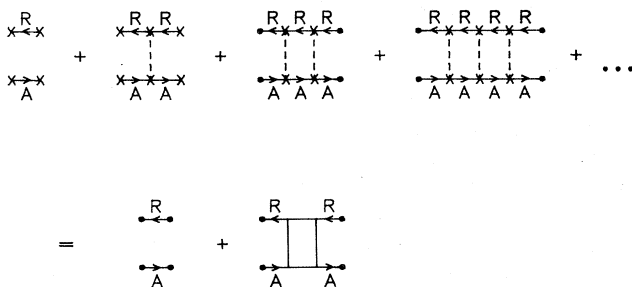


FIG. 17. The diagrammatic representation of the diffusion process.

quantum-mechanical interference between amplitudes for waves traversing closed classical diffusion loops in opposite directions, as depicted in Fig. 18. In Fig. 18 the solid line corresponds to the retarded line in Fig. 16, and the broken line to the advanced line, or, equivalently, the complex conjugate of the amplitude for transversing the loop in the opposite direction. The maximally crossed diagrams thus describe the interference part of the probability for the electron in a random medium to be scattered back to its source. In the momentum representation the Cooperon describes the singular contribution that arises when the momenta of the Green's functions are opposite, whereas the Diffuson singularity comes when the difference of the momenta is small. The weak-localization phenomenon is therefore also referred to as coherent backscattering. In a time-reversal-invariant situation the amplitudes for traversing a closed loop in opposite directions are identical, and for such a coherent situation one must trace the complete interference pattern of wave reflection in a random medium, where one encounters the phenomenon of localization (Anderson, 1958). The above standard impurity averaging technique is insufficient to trace the complete wave pattern. For such an accomplishment the impurity average must be performed from the outset, and one is led to the field-theoretic description of transport properties; for the impurity case this reduces to the nonlinear sigma model (Wegner, 1979; Efetov, 1984). The renormalization-group technique can then be applied, thus making an interesting connection between transport theory and the theory of phase transitions. In order to get a finite result for the first quantum correction to the conductance at zero temperature, we therefore need to consider a time-dependent external field which will give us a valid perturbative result in the expansion parameter $1/k_F l$. The first quantum correction leads to a smaller conductance, exhibiting the precursor effect of localization, the weak-localization regime. An elegant and physical description of the weak-localization effect, based on a detailed description of the tracing of backscattered waves, has been given by Chakravarty and Schmid (1986).

The coherence between pairs of time-reversed trajectories is interrupted when the environment, besides the dominating random potential, is taken into account. At nonzero temperatures energy exchange due to interaction with the environment will partially upset the particular

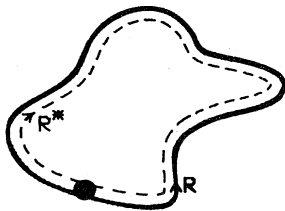


FIG. 18. The quantum interference process giving rise to the weak-localization effect is reflected in the two possible ways a diffusive loop can be transversed.

coherence between time-reversed paths involved in the weak-localization phenomena. The effects of electron-electron interactions (Altshuler, Aronov, and Khmel'nitskii, 1982) and electron-phonon interactions (Rammer and Schmid, 1986), have been studied in detail theoretically, and can be adequately accounted for by introducing a phase-breaking rate $1/\tau_\phi$ in the equation for the Cooperon, Eq. (5.42), describing its exponential decay in the long-time limit. A comprehensive understanding of the length scale $L_\phi = \sqrt{D\tau_\phi}$ over which the electron diffuses quantum mechanically coherently has been established and has given valuable information on inelastic scattering. The phase coherence length L_ϕ at low temperatures is much larger than the impurity mean free path l , explaining the slow spatial variation of the Cooperon on the scale of the mean free path, which we have repeatedly exploited.

The basic feature of the interaction effects can be understood by the observation that the single-particle Green's function will be additionally damped due to interactions, resulting in the substitution in Eq. (5.32) $1/\tau \rightarrow 1/\tau + 1/\tau_{in}$, where $1/\tau_{in}$ is the inelastic scattering rate. This will in turn lead to the change in the Cooperon equation, Eq. (5.42), $\omega \rightarrow \omega + i/\tau_{in}$. In most cases the inelastic scattering rate $1/\tau_{in}$ is identical to the phase-breaking rate $1/\tau_\phi$, as for example in the case of electron-phonon interaction (Rammer and Schmid, 1986). However, one should keep in mind that the inelastic scattering rate is not defined through a physically measurable quantity, but is a useful estimate, and all energy transfers are weighted equally, whereas for phase breaking, processes with small energy transfers, $\hbar\omega < \hbar/\tau_\phi$, are inefficient in destroying the phase coherence between time-reversed trajectories of duration less than the phase coherence time τ_ϕ . In terms of the diagrams this is reflected by the fact that interaction lines can connect the upper and lower particle lines in the Cooperon, whereas there is no such process for the inelastic scattering rate (Aronov, 1984). This is of importance in the case of a thin film, the quasi-two-dimensional case, where there are multiple scatterings with small energy transfer due to electron-electron interaction (Altshuler, Aronov, and Khmel'nitskii, 1982; Eiler, 1984). Calculating the phase-breaking rate is, however, closely related to calculating interaction effects in disordered metals. For general reviews on interaction effects we refer the reader to Altshuler and Aronov (1985) and Schmid (1985).

From an experimental point of view the breaking of time-reversal invariance by an externally controllable magnetic field in the low-field regime, where classical magnetoresistance is absent, is the tool by which to study the weak-localization effect and obtain important information on inelastic scattering times. Magnetoresistance measurements in the weak-localization regime have considerably enhanced the available information regarding inelastic scattering times (Bergmann, 1984). The influence of a magnetic field on the Cooperon is readily

established in view of the already presented formulas. In the weak magnetic field limit, $l^2 < l_B^2$, where $l_B = (\hbar/2|e|B)^{1/2}$ is the magnetic length, we can neglect the Landau quantization of the electronic motion and obtain, as in the field-free case, Eq. (5.36). The Green's function in the presence of such a weak magnetic field is then described by the line integral of the vector potential \mathbf{A} and, according to Eq. (3.11), changed by the additional action due to the magnetic field,

$$G_\epsilon^R(\mathbf{x}, \mathbf{x}') \rightarrow G_\epsilon^R(\mathbf{x}, \mathbf{x}') \exp \left[\frac{ie}{\hbar} \int_{\mathbf{x}'}^{\mathbf{x}} d\mathbf{l} \cdot \mathbf{A}(\mathbf{l}) \right], \quad (5.46)$$

resulting in the change

$$\tilde{J}_\omega^C(\mathbf{x}, \mathbf{x}') \rightarrow \tilde{J}_\omega^C(\mathbf{x}, \mathbf{x}') \exp \left[\frac{2ie}{\hbar} \int_{\mathbf{x}'}^{\mathbf{x}} d\mathbf{l} \cdot \mathbf{A}(\mathbf{l}) \right]. \quad (5.47)$$

Repeating the Taylor expansion leading to Eq. (5.39), we now obtain in the Cooperon equation additional terms due to the presence of the magnetic field (Al'tshuler *et al.*, 1980),

$$\left[-i\omega - D \left[\nabla_{\mathbf{x}} - \frac{2ie}{\hbar} \mathbf{A}(\mathbf{x}) \right]^2 + 1/\tau_\phi \right] C_\omega(\mathbf{x}, \mathbf{x}') = \frac{1}{\tau} \delta(\mathbf{x} - \mathbf{x}'). \quad (5.48)$$

Here we have inserted the phase-breaking rate for whose detailed derivation we refer the reader to the above references. Since the magnetic field itself influences the phase coherence, the phase-breaking rate can be influenced by the magnetic field. This is of importance in the quasi-two-dimensional case where the quasi-elastic electron-electron scattering gives the dominant contribution to the phase-breaking rate (Eiler, 1985). The theory of weak localization can be conveniently formulated in the quasiclassical Green's-function scheme (Rammer, 1985), which is particularly useful for treating time-dependent fields.

The Cooperon equation (5.48) is, according to Eq. (3.8), identical to the equation for the Green's function for a fictitious particle with mass equal to $1/2D$ and charge $2e$ in a magnetic field. The well-known solution of the Schrödinger equation for a particle in a magnetic field in terms of the Landau states allows us to write down, analogously to Eq. (5.19), an expression for the Cooperon in the presence of a magnetic field of strength B and direction perpendicular to a film of thickness a (we can now safely assume that the external electric field is static, so that its frequency is equal to zero, $\omega = 0$),

$$C_0(\mathbf{x}, \mathbf{x}') = \frac{1}{a} \sum_{n,k} \frac{\psi_{nk}^*(\mathbf{x}') \psi_{nk}(\mathbf{x})}{-4DeB\tau\hbar^{-1}(n + \frac{1}{2}) + \tau/\tau_\phi}. \quad (5.49)$$

Here ψ_{nk} are the Landau wave functions (Landau and Lifshitz, 1965), where n is the orbital quantum number and k the quantum number describing the position of the orbit. The three-dimensional case can be treated similar-

ly (Kawabata, 1980), but there the anomalous magnetoresistance is less pronounced.⁷

The quantum number describing the motion along the magnetic field has dropped out of Eq. (5.49), since only the term with lowest value, equal to zero, contributes, provided the thickness of the film is smaller than the phase coherence length, $a < L_\phi$, the thin film, or quasi-two-dimensional criterion, in conjunction with the weak restriction $a < l_B$. In the case of pure films where the elastic scattering is dominated by the surface scattering, $l > a$, the above diffusive description must be abandoned in favor of the Boltzmann type (Dugaev and Khmel'nitskii, 1984). We have in Eq. (5.49) safely assumed that the external electric field is static, so that its frequency is equal to zero, $\omega = 0$, since the magnetic field is seen to cut off the singularity in the Cooperon, thus depressing the tendency to localization. We should therefore expect Eq. (5.49) to lead to a positive magnetoconductivity. In accordance with the derivation of the Cooperon equation (5.48), we can only describe variations on length scales larger than the mean free path, so that the sum over orbital quantum number n in Eq. (5.49) should terminate at values of the order l_B^2/l^2 . The magnetoconductance of a thin film is now obtained by inserting Eq. (5.49) into Eq. (5.36) and subtracting the zero-field conductance. When we utilize the series representation of the digamma function ψ (Gradshteyn and Ryzhik, 1980), the low-field magnetoconductance of a thin film has the form (Al'tshuler, Aronov, Larkin and Khmel'nitskii, 1981)

$$\delta \langle G_{\alpha\beta}^{(B)} \rangle = \langle G_{\alpha\beta}^{(B)} \rangle - \langle G_{\alpha\beta}^{(0)} \rangle = \frac{e^2}{4\pi^2\hbar} f(4D|e|B\hbar^{-1}\tau_\phi) \delta_{\alpha\beta}, \quad (5.50)$$

where the function f is given by

$$f(x) = \ln x + \psi(1/2 + 1/x). \quad (5.51)$$

The magnetoconductance is seen to have a quadratic upturn at low fields and to saturate beyond a characteristic field of the order of $\hbar/|e|D\tau_\phi$.

In the above derivation we assumed that the magnetic field is weak, that is, the cyclotron frequency, $\omega_c = |e|B/m$, is much smaller than the inverse mean free time $1/\tau$: $\omega_c\tau < \hbar/\epsilon_F\tau$. From Eq. (5.49) or Eq. (5.50) we see that the weak-localization magnetoconductance is sensitive to very small magnetic fields, namely, fields for which the magnetic length becomes comparable to the phase coherence length, $l_B \sim L_\phi$, or equivalently, $\omega_c\tau \sim \hbar/\epsilon_F\tau_\phi$. Since the impurity mean free time τ can

⁷In the strictly one-dimensional case there is no weak-localization regime due to the absence of the small expansion parameter, which in general is given by $(k_F l)^{1-d}$. However, in the one-dimensional case methods are available that can give exact results (Berezinskii, 1974; Abrikosov and Ryzhkin, 1978).

be much smaller than the phase coherence time τ_ϕ , the above description can be valid over a wide magnetic-field range where classical magnetoconductance effects are absent, since they are governed by the orbit-bending scale, $\omega_c \tau \sim 1$, whereas the above quantum effect sets in when a loop of typical area L_ϕ^2 encloses a flux quantum. Beyond this low-field limit, the expression for the magnetoconductance cannot be given in closed form, and its derivation is more involved, since we must account for the orbit bending of the magnetic field (Kawabata, 1984). When the impurity mean free time τ becomes comparable to the phase coherence time τ_ϕ , we are no longer in the diffusive regime, and a Boltzmann-type description must be introduced (Wittmann and Schmid, 1987).

According to Eq. (5.50) the magnetoconductance is positive, which is a distinct sign that the effect is not classical. Any magnetoconductance calculated on the basis of the Boltzmann equation is negative. The positive magnetoconductance can be understood qualitatively from the geometrical properties of diffusion in two dimensions. The presence of the magnetic field breaks time-reversal invariance and partially upsets the identity of phase factors for time-reversed paths, so that the negative contribution from each loop in the impurity field to the conductance is, in accordance with the phase-shift prescription for amplitudes, Eq. (5.46), now multiplied by an oscillatory factor

$$\begin{aligned} \langle G(B) \rangle - \langle G(0) \rangle &= \frac{e^2}{4\pi^2 \hbar} \left\langle \sum_c [1 - \cos(2\pi\Phi_c/\Phi_0)] e^{-t_c/\tau_\phi} \right\rangle. \end{aligned} \quad (5.52)$$

The summation in Eq. (5.52) is over all loops; that is, the closed classical orbits in the random potential returning to within a mean free path to a given point, and t_c is the duration for transversing loop c ; Φ_c is the enclosed flux of loop c , and Φ_0 the flux quantum $\Phi_0 = h/2|e|$. The sum in Eq. (5.52) should be weighted with the probability for the closed classical loop, which we express by the brackets. In weak magnetic fields, only the longest loops are influenced by the phase shift due to the magnetic field [loops that are longer than the phase coherence length are not counted, as their coherence is destroyed by inelastic scattering according to Eq. (5.52)]. It is evident from Eq. (5.52) that the low-field magnetoconductance is positive and quadratic in the field. The continuing positive magnetoconductance is, however, simply a geometric property of diffusion, namely, that small loops are prolific. In the present two-dimensional case the number of closed loops is inversely proportional to their area.

We shall not describe the theory of weak localization any further, as our aim was to show that the effect can be described in quantitative manner by the elementary method we have introduced, thus providing a simple connection between the formal treatments (Al'tshuler, Aronov, Khmel'nitskii, and Larkin, 1982; Lee and Ramakrishnan, 1985) and the more intuitive description of

Chakravarty and Schmid (1986). We shall, however, mention the many further interesting quantum effects due to weak localization in solids, which can be described by the presented single-particle approach. The weak-localization Aharonov-Bohm effect in multiply connected macroscopic samples, such as a cylinder, is an illuminating manifestation of the quantum interference feature of weak localization (Al'tshuler, Aronov, and Spivak, 1981; Al'tshuler, Aronov, Spivak, Sharvin, and Sharvin, 1982; Aronov and Sharvin, 1987), as is the Andreev-reflection-induced sensitivity of the conduction properties of a normal conductor to the phase difference of the order parameter of two surrounding superconductors in a SNS junction (Spivak and Khmel'nitskii, 1982). Additional important phase-breaking and scattering mechanisms not dealt with here are phase breaking due to superconducting fluctuations (Larkin, 1980; Gordon, 1984; Brenig *et al.*, 1986); the effect of spin-flip and spin-orbit scattering (Hikami *et al.*, 1980), the latter leading to the phenomenon of weak antilocalization; suppression of weak-localization effects by electromagnetic radiation (Al'tshuler, Aronov, and Khmel'nitskii, 1981; Fal'ko, 1987; Wang and Lindelof, 1987; Vitkalov *et al.*, 1988); magnetoresistance in a longitudinal magnetic field (Al'tshuler and Aronov, 1981); weak localization in inhomogeneous magnetic fields (Rammer and Shelankov, 1987; Geim, 1989; Bending *et al.*, 1990); and weak localization of electrons in a classical gas (Afonin *et al.*, 1987).

We close this section by noting that the weak-localization phenomenon is a general feature of wave propagation in random media, be the wave nature of classical origin, such as light and sound, or quantum origin. The effect was in fact investigated in connection with multiple scattering of electromagnetic waves (Watson, 1969). It is amusing that it took the quantum nature of electronic motion to understand the fundamentals of the problem and to develop the formalism for quantitative calculations. For a recent set of reviews on classical wave propagation in random media we refer the reader to the book edited by Shen (1989).

D. Landauer conductance formula

In the preceding section on weak localization we discussed the first quantum correction to the macroscopic transport properties of disordered conductors. In the macroscopic limit only the average properties of a sample manifest themselves. Thus a macroscopic sample can be adequately discussed in terms of the impurity-averaged density matrix and characterized by a single average quantity, the impurity mean free path. However, with today's fabrication technology it is possible to produce samples that exhibit their unique impurity configurations. Such samples are in the realm between the microscopic level, set by the elastic mean free path, and the macroscopic level, set by the phase coherence length, and exhibit so-called mesoscopic phenomena.

Mesoscopic phenomena show up when inelastic scattering is weak, allowing the phase coherence length to exceed the sample size, and thus enabling quantum interference to take place throughout the sample. In the mesoscopic regime an average quantity is insufficient for characterizing a sample. Sample-specific “fingerprints” of the impurity configuration, such as the noiselike oscillations in the magnetoconductance, will manifest themselves in the universal conductance fluctuations (Al’tshuler, 1985; Lee and Stone, 1985).

A quite different approach to quantum transport due to Landauer (1957, 1970, 1985) has played an important role in the development of mesoscopic physics (Imry, 1986). In the conventional Hamiltonian approach, as presented in the preceding sections, the current is calculated as the response to an external field. However, since only elastic scattering takes place in the sample region, the transport problem can equally well be viewed as a scattering problem, where the current is the externally fixed quantity; in fact, it is the typical control parameter for experiments.

In the previous discussion of the conductance of macroscopic samples, we did not need to address the question of the actual measurement situation, such as the presence of leads and the manufacturing of the external field. This is not the case for mesoscopic phenomena, since there the extension of quantum-mechanical coherence defines the sample extension and is not an artificial distinction imposed on our part (Benoit *et al.*, 1987; Skocpol *et al.*, 1987).

Now, by imposing the same physical conditions as in the Landauer approach, we shall see how the linear-response expression for the conductance reduces to a Landauer-type expression. In the Landauer approach the transport process is viewed as the scattering of impinging charges from incoherent current sources, reservoirs, off an obstacle, the disordered region, whose properties are completely characterized by its reflection and transmission coefficients. An expression for the conductance is then obtained by counting the net charge flux from current sources at different chemical potentials. In the linear response approach as presented above, we shall assume that the disordered region is attached to two perfect leads, that is, disorder-free regions, as depicted in Fig. 19. In view of the counting strategy underlying the Landauer approach, we integrate the current density, Eq. (5.20), over a cross section S far out in one of the leads, say the right one, at position x , giving the current in the right lead

$$I(x) = \int_S d\mathbf{s} \cdot \mathbf{j}(\mathbf{x}) = \int d\mathbf{x}' \int_S d\mathbf{s} \cdot \vec{\sigma}(\mathbf{x}, \mathbf{x}') \cdot \mathbf{E}(\mathbf{x}') . \quad (5.53)$$

We shall be interested in the dc case, and shall henceforth delete the external frequency $\omega=0$ from the formulas. As depicted in Fig. 19 the x direction is chosen along the leads. Writing the electric field \mathbf{E} as the gradient of the scalar potential ϕ , $\mathbf{E} = -\nabla\phi$, and using the diver-

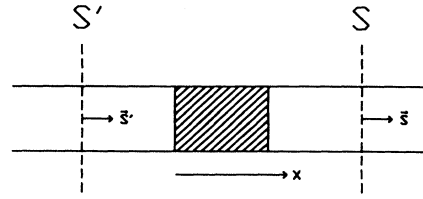


FIG. 19. The schematics of a disordered region attached to perfect leads.

gence theorem we obtain

$$I(x) = \int d\mathbf{x}' \int_S d\mathbf{s} \cdot \vec{\sigma}(\mathbf{x}, \mathbf{x}') \cdot \vec{\nabla}_{\mathbf{x}'} \phi(\mathbf{x}') - \int_{S'} \phi(\mathbf{x}') \int_S d\mathbf{s} \cdot \vec{\sigma}(\mathbf{x}, \mathbf{x}') \cdot d\mathbf{s}' . \quad (5.54)$$

The first term in Eq. (5.54) can be shown to be zero by explicitly differentiating the conductivity tensor, $\sigma(\mathbf{x}, \mathbf{x}') \cdot \vec{\nabla}_{\mathbf{x}'} = 0$, as is generally true due to charge conservation (Martin and Schwinger, 1959). In the present case of impurity scattering the identity is readily established (Kane, Serota, and Lee, 1988), according to Eq. (5.21), by repeated use of the equation of motion for the Green’s function

$$(\epsilon - H_0)G^R(\mathbf{x}, \mathbf{x}'; \epsilon) = \hbar\delta(\mathbf{x} - \mathbf{x}') , \quad (5.55)$$

where H_0 is the Hamiltonian for the particle in the impurity field and the confining potential defining the sample and leads.

From the symmetry property of the conductivity tensor

$$\sigma_{\alpha\beta}(\mathbf{x}, \mathbf{x}') = \sigma_{\beta\alpha}(\mathbf{x}', \mathbf{x}) , \quad (5.56)$$

which can be immediately read off from Eq. (5.21), we therefore also have

$$\nabla_{\mathbf{x}} \cdot \vec{\sigma}(\mathbf{x}, \mathbf{x}') = 0 . \quad (5.57)$$

The non-divergence of the conductivity tensor reflects charge conservation and is, for the considered dc case, according to Eq. (5.20), equivalent to the statement that the divergence of the current density is zero, $\nabla \cdot \mathbf{j} = 0$, or, equivalently, that the current in the lead does not depend on the position x of the chosen cross section, so that $I(x)$ in Eq. (5.53), in fact, is independent of position once we are out in the lead. According to Eq. (5.53), the volume integration merely has to enclose the spatial region where the electric field is nonzero. Choosing the corresponding enclosing surface S' to lie far away from the sample and gauging the potential to be zero in the left lead and $-U$ in the right lead, that is, choosing the direction from left to right as the positive current direction, we obtain from Eq. (5.54) for the current in the leads

$$I = U \int_{S'} \int_S d\mathbf{s} \cdot \vec{\sigma}(\mathbf{x}, \mathbf{x}') \cdot d\mathbf{s}' . \quad (5.58)$$

In the derivation above we calculated the current in the right lead. However, as noted above, by interchanging

the introduction of the surfaces S and S' , we could of course obtain the same expression (5.58), for the current in the left lead, as is evident from the symmetry of Eq. (5.58). We therefore have for the conductance

$$G = \int_S \int_{S'} d\mathbf{s} \cdot \vec{\sigma}(\mathbf{x}, \mathbf{x}') \cdot d\mathbf{s}' \\ = \int_S d\rho \int_{S'} d\rho' \sigma_{xx}(\mathbf{x}, \mathbf{x}') . \quad (5.59)$$

$$G = -\frac{e^2 \hbar}{8\pi m^2} \operatorname{Re} \int_{-\infty}^{\infty} d\epsilon \left[-\frac{\partial f}{\partial \epsilon} \right] \int_S d\rho \int_{S'} d\rho' , \\ \times \left[\left[\frac{\partial^2}{\partial x \partial x'} [G^R(\mathbf{x}, \mathbf{x}'; \epsilon) - G^A(\mathbf{x}, \mathbf{x}'; \epsilon)] \right] (G^R(\mathbf{x}', \mathbf{x}; \epsilon) - G^A(\mathbf{x}', \mathbf{x}; \epsilon)) \right. \\ \left. - \left[\frac{\partial}{\partial x} [G^R(\mathbf{x}, \mathbf{x}'; \epsilon) - G^A(\mathbf{x}, \mathbf{x}'; \epsilon)] \right] \left[\frac{\partial}{\partial x'} [G^R(\mathbf{x}', \mathbf{x}; \epsilon) - G^A(\mathbf{x}', \mathbf{x}; \epsilon)] \right] \right] . \quad (5.60)$$

The retarded Green's function $G^R(\mathbf{x}, \mathbf{x}', \epsilon)$ is, according to its definition, the component of the wave function, for energy ϵ , at the cross section S in the right lead for a point-source emitter in the cross-sectional plane S' in the left lead. In the leads the Green's function therefore has the asymptotic expansion in terms of outgoing waves

$$G^R(\mathbf{x}, \mathbf{x}'; \epsilon) = \sum_{l,r} \tilde{t}_{rl}^\epsilon [\chi_l(\rho') e^{-ik_r^\epsilon x'}]^* \chi_r(\rho) e^{ik_r^\epsilon x} , \quad (5.61)$$

where χ_r denotes the transverse, r -channel wave function in the right lead, and similarly for the left lead. The wave vector in the propagating direction in the right lead, k_r^ϵ , corresponding to total energy ϵ and transverse mode r , satisfies $(\hbar k_r^\epsilon)^2/2m = \epsilon - \epsilon_r$, where ϵ_r is the transverse-mode energy, and similarly for the left lead.

$$\int d\rho \int d\rho' \left[\left[\frac{\partial^2 G^R(\mathbf{x}, \mathbf{x}'; \epsilon)}{\partial x \partial x'} \right] G^R(\mathbf{x}', \mathbf{x}; \epsilon) - \left[\frac{\partial G^R(\mathbf{x}, \mathbf{x}'; \epsilon)}{\partial x} \right] \left[\frac{\partial G^R(\mathbf{x}', \mathbf{x}; \epsilon)}{\partial x'} \right] \right] = -2 \sum_{l,r} k_l^\epsilon k_r^\epsilon \tilde{t}_{rl}^\epsilon \tilde{t}_{lr}^\epsilon . \quad (5.63)$$

The transmission amplitude, which we denote by t_{rl} , is the amplitude for propagation from channel state l in the left lead to channel state r in the right lead, and therefore given by the corresponding matrix element

$$t_{rl}^\epsilon = \frac{\hbar \sqrt{k_l^\epsilon k_r^\epsilon}}{m} e^{-ik_l^\epsilon x - ik_r^\epsilon x'} \\ \times \int d\rho \int d\rho' \chi_r^*(\rho) G^R(\mathbf{x}, \mathbf{x}'; \epsilon) \chi_l(\rho') . \quad (5.64)$$

In the Landauer approach all modes up to the Fermi level are populated by the current reservoir, emitting electrons towards the sample. This corresponds to the usual normalization condition of scattering theory that

The vectors ρ and ρ' denote the two-dimensional vectors in the cross-sectional planes S and S' , respectively, $\mathbf{x} = (x, \rho)$. That the conductance is a real number is reflected by the existence of pairs in Eq. (5.59) that, if written out explicitly according to Eq. (5.21), are each other's complex conjugates, due to Eq. (2.31), so that we can in fact write Eq. (5.59) as

Using the expansion (5.61) and the property (2.31), one readily verifies the identity

$$\int d\rho \left[\left[\frac{\partial^2 G^R(\mathbf{x}, \mathbf{x}'; \epsilon)}{\partial x \partial x'} \right] G^A(\mathbf{x}', \mathbf{x}; \epsilon) \right. \\ \left. - \left[\frac{\partial G^R(\mathbf{x}, \mathbf{x}'; \epsilon)}{\partial x} \right] \left[\frac{\partial G^A(\mathbf{x}', \mathbf{x}; \epsilon)}{\partial x'} \right] \right] = 0 , \quad (5.62)$$

and similarly for R and A interchanged. For the remaining terms we need only consider two of them, since the other two are accounted for by simply interchanging variables. Again, using the asymptotic expansion of the Green's function, Eq. (5.61), we find by using the orthogonality of the channel states that the remaining terms add,

each channel carries unit flux. Inserting Eq. (5.61) into Eq. (5.64) we obtain the relationship between the transmission amplitudes and the expansion coefficients in Eq. (5.61), $mt_{rl}^\epsilon = \hbar \sqrt{k_l^\epsilon k_r^\epsilon} \tilde{t}_{rl}^\epsilon$. Making use of the fact that $t_{rl}^\epsilon = (t_{lr}^\epsilon)^*$ by time-reversal invariance, we obtain the scattering formula for the conductance

$$G = \frac{e^2}{4\pi \hbar} \int_{-\infty}^{\infty} d\epsilon \left[-\frac{\partial f}{\partial \epsilon} \right] \sum_{l,r} (|t_{lr}^\epsilon|^2 + |t_{rl}^\epsilon|^2) \\ = \frac{e^2}{2\pi \hbar} \int_{-\infty}^{\infty} d\epsilon \left[-\frac{\partial f}{\partial \epsilon} \right] \sum_{l,r} |t_{rl}^\epsilon|^2 , \quad (5.65)$$

in agreement with Fisher and Lee (1981).

In the above two-probe situation the leads, with the imposed boundary condition, adequately function as the reservoirs of the Landauer approach, ensuring that an electron never reenters the sample without having its phase randomized. The conductance formula (5.65) applies, therefore, according to its derivation, to coherent wave propagation between two phase-randomizing reservoirs. The conductance formula (5.65) differs from the original Landauer formula (Landauer, 1957, 1970, 1985), which relates the current in a four-probe measurement to the chemical potentials of completely phase-randomizing voltage probes eliminating interference between incoming currents (Engquist and Anderson, 1981). The derivation of the original Landauer formula from linear-response theory similarly attributes an effective chemical potential to the leads (Thouless, 1981; Langreth and Abrahams, 1981). In the realm of mesoscopics there is no possibility for a distinction between the phase-randomizing properties of current and voltage leads, and they should accordingly be treated on an equal footing. The obstacle giving rise to scattering need not be an impurity configuration; scattering can also originate simply from the geometry of the sample, as in the case of constrictions showing quantized resistance steps (van Wees *et al.*, 1988). The conductance formula for the present two-probe case, Eq. (5.65), as well as its generalization to an arbitrary number of probes can be derived using the Landauer approach (Büttiker, 1986a, 1986b) and further generalized to include a magnetic field, as is necessary for a discussion of the Hall effect (Büttiker, 1988). The derivation of the scattering formulas from linear-response theory can be generalized to the case of an arbitrary number of probes with the inclusion of a magnetic field (Baranger and Stone, 1989).

In addition to making contact between the Landauer approach to quantum transport and linear-response theory, Eq. (5.65) paves the way for treating situations in which inelastic scattering within the sample is non-negligible. Such situations pose no problem in principle in the linear-response approach, whereas in the intuitively appealing but heuristic Landauer approach a realistic inclusion of these processes is less obvious. A description within linear response that includes the effect of linear coupling to an environment has been given by Feng (1990).

Just as in the present section, we shall in the following be interested in the conductance of a specific sample. Clearly, a complete description is impossible and unwarranted when the sample contains many impurities. In the Landauer approach in such cases one can with benefit treat the transmission coefficients in the equation for the conductance as phenomenological parameters. In cases where the impurity scattering is weak or solely due to geometry, so that the mean free path exceeds the sample length, $l > L$ (the ballistic regime), one can in fact calculate the relevant transmission coefficients analytically for special cases, such as for a smooth constriction (Glazman

et al., 1988), and for other geometries use the scattering formula (5.65) as a starting point for a numerical solution (Datta, 1989; Ravenhall, 1989; Sols *et al.*, 1989; Stone, 1989). For samples containing many impurities, however, one is only interested in obtaining a statistical characterization of the sample-to-sample variations. In the following section we give a simple demonstration of how such statistical information can be obtained by use of the standard diagram technique.

E. Conductance fluctuations

Quite recently it has been realized that due to quantum interference effects a sample will exhibit its individuality on length scales much larger than expected; at zero temperature this scale is in fact infinite. Thanks to the advances in fabrication of microstructures it has therefore been possible in recent years to produce samples that reflect individual differences due to their specific impurity configurations. An estimate shows that at temperatures of the order of a few Kelvins the sample size should be in the micrometer range or smaller. In the following we shall show that, when the extension of a sample becomes comparable to the phase coherence length, the individuality of the sample will be manifest in its physical properties. Such a sample is said to be mesoscopic. Characteristically the conductance will exhibit sample-specific, noiselike but reproducible oscillations as a function of, say, magnetic field or chemical potential (Umbach *et al.*, 1984; Stone, 1985; Webb *et al.*, 1985; Washburn and Webb, 1986). The sample behavior is thus no longer characterized by its average characteristics, such as the average conductance or impurity concentration. The statistical assumption of phase-incoherent and therefore independent subsystems, allowing for such an average description, is no longer valid when the transport takes place quantum mechanically coherently throughout the whole sample. As a consequence, mesoscopic samples do not possess the property of being self-averaging, that is, the relative fluctuations do not vanish in a central-limit fashion inversely proportional to the volume in the large-volume limit. To describe the fluctuations from the average value we need to study the higher moments of the conductance distribution such as the variance $\Delta G_{\alpha\beta,\gamma\delta}$ (Al'tshuler, 1985; Lee and Stone, 1985),

$$\Delta G_{\alpha\beta,\gamma\delta} = \langle (G_{\alpha\beta} - \langle G_{\alpha\beta} \rangle)(G_{\gamma\delta} - \langle G_{\gamma\delta} \rangle) \rangle. \quad (5.66)$$

The diagrams for the variance can still be managed with the standard impurity diagram technique, and a typical conductance fluctuation diagram is depicted in Fig. 20, where the box denotes the Diffuson as in Fig. 17. The construction of the conductance fluctuation diagrams follows from the conductivity equation (5.21): Draw two different conductance diagrams like the first diagram of Fig. 14, but with the propagators including the impurity

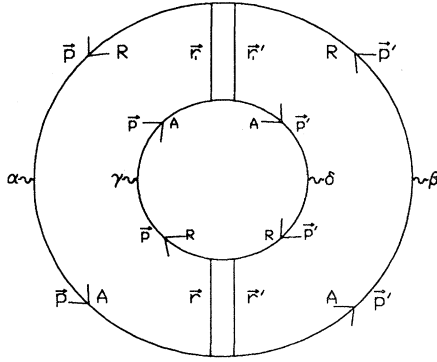


FIG. 20. Typical conductance fluctuation diagram.

scattering. Treating the impurity scattering perturbatively, we get impurity vertices, which we have to pair in all possible ways. Since we subtract the squared average conductance in forming the variance ΔG , the diagrams for the variance consist only of diagrams in which the two conductance loops are connected by impurity lines. As already noted in the discussion of weak localization, the dominant contributions to such loop-type diagrams are from the infrared, long-wavelength divergence of the Diffuson or Cooperon,

$$D_{\omega}(\mathbf{q}) = \frac{1/\tau}{i\omega + Dq^2} = C_{\omega}(\mathbf{q}), \quad (5.67)$$

as obtained by Fourier transformation of Eq. (5.42).

To calculate the contribution to the variance from the diagram in Fig. 20, we first imagine writing the corresponding expression down in the spatial representation in accordance with the usual rules for conductance diagrams, as specified by the conductivity tensor (5.21) and the conductance as in Eq. (5.23), but for the unaveraged conductance. If we assume that the sample dimensions are bigger than the impurity mean free path, $L > l$, the spatial extension of the integration over the external, excitation and measuring, vertices is essentially infinite, since the propagators have the spatial extension of the mean free path, according to Eq. (5.33). We can therefore introduce the Fourier transform, Eq. (5.32), for the propagators, since no reference to the finiteness of the system is necessary for such local quantities. Furthermore, because of the long-range spatial character of the Diffuson, we can set the spatial labels in the Diffusons in Fig. 20 equal to each other: that is, $\mathbf{r}_1 = \mathbf{r}$ and $\mathbf{r}'_1 = \mathbf{r}'$. All the spatial integrations, except those determined by the Diffuson, can then be performed, leading to the momentum labels for the propagators depicted in Fig. 20. Let us study the fluctuations in the dc conductance where the frequency ω of the external field is zero. The energy labels have for visual clarity been deleted from Fig. 20, since we have only elastic scattering and therefore one label, say ϵ , for the outer ring and one for the inner, ϵ' . According to the Feynman rules, we obtain for the diagram in Fig. 20 the following analytical expression:

$$\begin{aligned} \langle G_{\alpha\beta} G_{\gamma\delta} \rangle_D = & L^{-4} \left[\frac{e^2 u^2}{4\pi\hbar^2 m^2} \right]^2 \int_{-\infty}^{\infty} d\epsilon \int_{-\infty}^{\infty} d\epsilon' \frac{\partial f}{\partial \epsilon} \frac{\partial f}{\partial \epsilon'} \int \frac{d\mathbf{p}}{(2\pi\hbar)^3} \int \frac{d\mathbf{p}'}{(2\pi\hbar)^3} p_{\alpha} p_{\gamma} p'_{\delta} p'_{\beta} \\ & \times G_{\epsilon}^R(\mathbf{p}') G_{\epsilon'}^A(\mathbf{p}') G_{\epsilon'}^A(\mathbf{p}') G_{\epsilon}^R(\mathbf{p}') G_{\epsilon}^R(\mathbf{p}) G_{\epsilon'}^A(\mathbf{p}) G_{\epsilon'}^R(\mathbf{p}) \int d\mathbf{r} \int d\mathbf{r}' |D_{\epsilon-\epsilon'}(\mathbf{r}, \mathbf{r}')|^2. \end{aligned} \quad (5.68)$$

In order to obtain Eq. (5.68), we have noted that

$$D_{\epsilon-\epsilon'}(\mathbf{r}, \mathbf{r}') = [D_{\epsilon-\epsilon'}(\mathbf{r}, \mathbf{r}')]^*, \quad (5.69)$$

which follows from the relationship between the retarded and advanced propagators, Eq. (2.31). At zero temperature, the Fermi functions are seen to set the energies in the Green's functions in the conductance loops to the Fermi energy, and the Diffuson frequency to zero. At zero temperature, therefore, we get for the diagram depicted in Fig. 20,

$$\begin{aligned} \langle G_{\alpha\beta} G_{\gamma\delta} \rangle_D = & L^{-4} \left[\frac{e^2 u^2}{4\pi\hbar^2 m^2} \right]^2 \int \frac{d\mathbf{p}}{(2\pi\hbar)^3} \int \frac{d\mathbf{p}'}{(2\pi\hbar)^3} p_{\alpha} p_{\gamma} p'_{\delta} p'_{\beta} \\ & \times [G_{\epsilon_F}^R(\mathbf{p}) G_{\epsilon_F}^A(\mathbf{p})]^2 [G_{\epsilon_F}^R(\mathbf{p}') G_{\epsilon_F}^A(\mathbf{p}')]^2 \int d\mathbf{r} \int d\mathbf{r}' |D_0(\mathbf{r}, \mathbf{r}')|^2. \end{aligned} \quad (5.70)$$

In the momentum representation the integration over all current vertices leads to momentum conservation at each vertex in the diagram, just as integration over time leads to energy conservation at each vertex.

It is important to note that the Diffuson appears with the same positions, or in the momentum representation with the same wave vector, twice. This is the leading

singularity we need to keep track of. If we try to construct variance diagrams containing, say three Diffusons, we will observe that they cannot have the same wave vector and thus give a contribution smaller by the factor of $1/\epsilon_F \tau$.

The momentum integrations at the current vertex can easily be calculated by the residue method,

$$j_{\alpha\gamma} = \int \frac{d\mathbf{p}}{(2\pi\hbar)^3} p_{\alpha} p_{\gamma} [G_{\epsilon_F}^R(\mathbf{p})]^2 [G_{\epsilon_F}^A(\mathbf{p})]^2 = \frac{4\pi}{3} \hbar p_F^2 N(\epsilon_F) \tau^3 \delta_{\alpha\gamma}, \quad (5.71)$$

and we obtain for the diagram in Fig. 20

$$\langle G_{\alpha\beta} G_{\gamma\delta} \rangle_D = L^{-4} \left[\frac{e^2 D \tau}{2\pi\hbar} \right]^2 \delta_{\alpha\gamma} \delta_{\delta\beta} \times \int d\mathbf{r} \int d\mathbf{r}' |D_0(\mathbf{r}, \mathbf{r}')|^2. \quad (5.72)$$

To calculate the Diffuson integrals we need to address the finite size of the sample and its attachment to the current leads, since at zero frequency the Diffuson has no inherent length-scale cutoff. At the surface where the sample, assumed to be a hypercube of length L , is attached to the leads, the Diffuson vanishes,

$$D_0(\mathbf{r}, \mathbf{r}') = 0, \quad \mathbf{r} \text{ or } \mathbf{r}' \text{ on lead surfaces}, \quad (5.73)$$

in accordance with the assumption that once the electron reaches the lead it never returns to the disordered-region phase coherently. On the other surfaces the current vanishes; that is, the normal derivative of the Diffuson must vanish,

$$\frac{\partial D(\mathbf{r}, \mathbf{r}')}{\partial \mathbf{n}} = 0, \quad \mathbf{r} \text{ or } \mathbf{r}' \text{ on nonlead surfaces} \\ \text{with surface normal } \mathbf{n}. \quad (5.74)$$

We shall assume, in accordance with the situation depicted in Fig. 19, that the leads have the same size as the sample surface. This thick-lead assumption can be relaxed, but due to the relationship between the fluctuations in the density of states and the time scale for diffusing out of the sample, that will in fact not change the results (Serota *et al.*, 1987). Solving the diffusion equation (5.42) for the Diffuson, with the above mixed boundary condition we obtain

$$\int d\mathbf{r} \int d\mathbf{r}' [D_0(\mathbf{r}, \mathbf{r}')]^2 = \left[\sum_n \frac{1/\tau}{D q_n^2} \right]^2, \quad (5.75)$$

where $n = (n_x, n_y, n_z)$ is the eigenvalue index in the three-dimensional case, and

$$q_{n_\alpha} = \frac{\pi}{L} n_\alpha, \quad n_\alpha = n_x, n_y, n_z, \\ n_x = 1, 2, \dots, \quad n_{y,z} = 0, 1, 2, \dots, \quad (5.76)$$

in accordance with the convention of Fig. 19 for the current leads. Lower dimensions correspond to neglecting the n_y and n_z 's. We therefore obtain from the diagram depicted in Fig. 20

$$\langle G_{\alpha\beta} G_{\gamma\delta} \rangle_D = \left[\frac{e^2}{2h} \right]^2 c_d \delta_{\alpha\gamma} \delta_{\delta\beta}, \quad (5.77)$$

where h is Planck's constant and the constant c_d depends on the sample dimension. The summation in Eq. (5.75)

should, in accordance with the validity of the diffusion regime, be restricted to values satisfying $n_x^2 + n_y^2 + n_z^2 \leq N$, where N is of the order of $(L/l)^2$. However, the sum converges rapidly and the constants C_d are seen to be of order unity. The dimensionality criterion is essentially the same as in the theory of weak localization, as we shall show in the discussion below of the physical origin of the fluctuation effects. The important thing to notice is that the long-range nature of the Diffuson provides the L^4 factor that makes the variance, average of the squared conductance, independent of sample size. The diagram depicted in Fig. 20 is only one of two possible pairings of the current vertices, and we obtain an additional contribution from the diagram in which, say, current vertices γ and δ are interchanged.

In addition to the contribution from the diagram in Fig. 20 there is another possible singular contribution to the variance from the diagram depicted in Fig. 21. This diagram contributes the same amount as the one in Fig. 20, but with a different pairing of the current vertices. We note that the diagram in Fig. 21 allows for only one assignment of current vertices. The contribution from the diagram in Fig. 20 can, through the Einstein relation, be ascribed to fluctuations in the diffusion constant, whereas the diagram in Fig. 21 gives the contribution from the fluctuations in the density of states, the two types of fluctuations being independent (Al'tshuler and Shklovskii, 1986).

Interchanging the retarded and advanced labels corresponding to the additional term in the conductivity tensor (5.21) gives rise to additional equal contributions. Furthermore, reversing the direction in one of the loops gives rise to similar diagrams, but now with the Cooperon appearing in Figs. 20 and 21 instead of the Diffuson. Because the boundary conditions on the Cooperon are the same, Eqs. (5.73) and (5.74), as for the Diffuson, in the absence of a magnetic field the Cooperon contributes an equal amount. For the total contribution to the variance of the conductance, we therefore have (allowing for

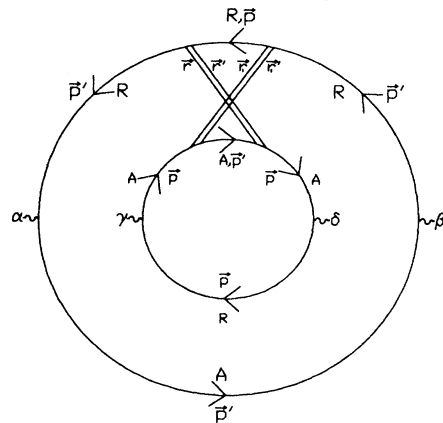


FIG. 21. Density-of-states-type fluctuation diagram contributing to the conductance fluctuations.

the spin degree of freedom of the electron would quadruple the value) at zero temperature

$$\Delta G_{\alpha\beta,\gamma\delta} = \left(\frac{e^2}{h}\right)^2 c_d (\delta_{\alpha\gamma}\delta_{\delta\beta} + \delta_{\alpha\delta}\delta_{\gamma\beta} + \delta_{\alpha\beta}\delta_{\gamma\delta}). \quad (5.78)$$

The variance of the conductance at zero temperature and for the chosen geometry, Eq. (5.78), is independent of the size and dimension of the sample and the degree of disorder, and the conductance fluctuations in the above metallic regime appear to be universal. However, for a noncubic sample, the variance will be geometry dependent (Al'tshuler and Khmel'nitskii, 1985; Lee *et al.*, 1987).

Since the average classical conductance, according to Eq. (5.35), is proportional to L^{d-2} , Ohm's law, we find that the relative variance $\Delta G / \langle G \rangle^2$ is proportional to L^{4-2d} . This result should be contrasted with the thermodynamic fluctuations, L^{-2d} , compared to which the quantum-interference-induced mesoscopic fluctuations are huge, reflecting the absence of self-averaging. The mesoscopic conductance fluctuations can be viewed as the volume average of the much larger local fluctuations in the current density (Aronov *et al.*, 1986). The local fluctuations reveal themselves in the large non-universal voltage or resistance fluctuations in multilead devices (Benoit *et al.*, 1987; Skocpol *et al.*, 1987; Baranger *et al.*, 1988; Hershfield and Ambegaokar, 1988; Kane, Lee, and DiVincenzo, 1988b; Hershfield, 1989).

The dominating role of the lowest eigenvalue in Eq. (5.75) indicates that mesoscopic fluctuations studied in situations with less invasive probes than the leads necessary for studying conductance fluctuations can be enhanced over the universal value. This is the case, for example, for the absorption fluctuations of a mesoscopic sample in an ac electric field (Serota *et al.*, 1987), or the fluctuations in ultrasonic attenuation (Serota, 1988). In the case of the conductance fluctuations, the necessary connection of the disordered region to the external preparation and measurement apparatus, battery and voltmeter, could simply be reduced to the functioning of the leads, which cut off the singularity in the Diffuson by the lowest eigenvalue, $n_x = 1$, reflecting the fact that due to the physical boundary conditions at the interface between sample and leads, the time scale for quantum interference processes to occur uninterrupted is the time it takes the electron to diffuse across the sample, L^2/D . Alternative ways of observing the mesoscopic fluctuations will in turn introduce the destruction of phase coherence, which is necessary for the experiment to function as a measuring device. With the discovery of the quantum interference effects discussed above, we thus encounter in solid state physics, in a rather practical matter, questions usually reserved for the quantum measurement problem (Wheeler and Zurek, 1980).

In order to understand the physical phenomena leading to Eq. (5.78) for the variance, we note that, just as the

conductance essentially is given by the probability for diffusing between points in the sample, the variance is likewise the product of two such probabilities. When we perform the impurity average, certain of the quantum interference terms will not be averaged away, since certain pairs of paths are coherent. This is similar in spirit to the case of coherence involved in the weak-localization effect, but in the present case of quite a different nature. For example, the quantum interference terms described by the diagram in Fig. 20 are depicted in Fig. 22, where the solid line corresponds to the outer conductance loop and the dashed line to the inner conductance loop. The wavy portion of the lines corresponds to the long-range diffusion process. When one takes the impurity average of the variance, the quantum interference terms can pair up for each diffusive path in the random potential, but now they correspond to amplitudes for propagation in different samples. The diagrams for the variance, therefore, do not describe any physical quantum interference process, as we are not describing a probability but a product of probabilities. The variance gives the statistical correlation between amplitudes in different samples. The interference term corresponding to the diagram in Fig. 21 is likewise depicted in Fig. 23. When a specific mesoscopic sample is considered, effectively no impurity average is performed as in the macroscopic case. The quantum interference terms in the conductance, which for a macroscopic sample averages to zero if we neglect the weak-localization effect, is therefore responsible for the mesoscopic fluctuations.

The result in Eq. (5.78) is valid in the metallic regime, where the average conductance is larger than e^2/h . To go beyond the metallic regime would necessitate introducing the quantum corrections to diffusion, the first of which is of the weak-localization type, which diagrammatically corresponds to inserting Cooperons in between Diffusons. Such an analysis is necessary for a study of fluctuations in a strongly disordered regime (Al'tshuler, Kravtsov, and Lerner, 1991).

The Diffuson and Cooperon in the conductance fluctuation diagrams do not describe diffusion and return probabilities, respectively, in a given sample, but quantum-statistical correlations between motion in

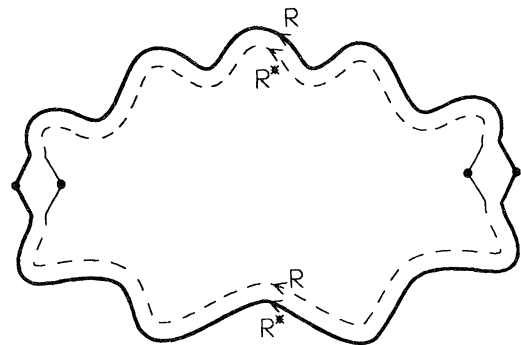


FIG. 22. The quantum interference process described by the fluctuation diagram in Fig. 20.

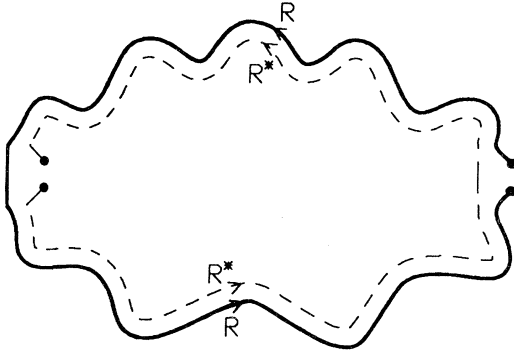


FIG. 23. The quantum interference process described by the fluctuation diagram in Fig. 21.

different samples, that is, different impurity configurations, as each conductance loop in Figs. 20 and 21 corresponds to different samples. In order to stress this important distinction, we shall in the following mark with tildes the Diffusons and Cooperons appearing as ladder diagrams in fluctuation diagrams.

We now briefly assess the effects of finite temperature. In addition to being temperature dependent due to the Fermi functions appearing in Eq. (5.68), the ladder diagrams will be modified by interaction effects. The presence of the Fermi functions corresponds to an energy average over the thermal layer near the Fermi surface, and through the energy dependence of the Diffuson and Cooperon introduces the temperature-dependent length scale $L_T = \sqrt{D\hbar/k_B T}$. Since the loops in the fluctuation diagrams correspond to different conductivity measurements, interaction lines (due for example, to, electron-phonon or electron-electron interaction) are not allowed to connect the loops in a fluctuation diagram. The diffusion pole of the Diffuson appearing in a fluctuation diagram is therefore not immune to interaction effects. This is only the case when the Diffuson describes diffusion within a sample, since, as we showed in the previous section, the diffusion pole is a consequence of particle conservation and therefore is unaffected by interaction effects. The consequence is that, just as in the case for the Cooperon, inelastic scattering will lead to a cutoff given by the phase-breaking rate $1/\tau_\phi$. In short, the temperature effects will therefore ensure that up to length scales near the phase coherence length the conductance fluctuations are determined by the zero-temperature expression, and beyond this scale the conductance of phase-incoherent volumes add, as in the classical case. A sample is therefore said to be mesoscopic when its size is in between the microscopic scale, set by the mean free path, and the macroscopic scale, set by the phase coherence length; $l < L < L_\phi$.

An important way to reveal the conductance fluctuations experimentally is to measure the magnetoresistance of a given sample. Since the conductance loops can correspond to samples placed in different field strengths, the diffusion pole appearing in a fluctuation diagram will not

be immune to the presence of magnetic fields, as in the case when the particle-hole ladder describes diffusion within a given sample, since particle conservation is, of course, unaffected by the presence of a magnetic field. To study fluctuation effects in magnetic fields, we must study the dependence of the variance on the magnetic fields $\Delta G_{\alpha\beta}(\mathbf{B}_+, \mathbf{B}_-)$, where \mathbf{B}_+ is the sum and \mathbf{B}_- the difference in the magnetic fields of the outer and inner loops. According to the low-field prescription for inclusion of magnetic fields. Eqs. (5.46) and (5.45), we get for the Diffuson

$$\left[D \left[-i\nabla - \frac{e}{\hbar} \mathbf{A}_-(\mathbf{x}) \right]^2 + 1/\tau_\phi \right] \tilde{D}_0(\mathbf{x}, \mathbf{x}') = \frac{1}{\tau} \delta(\mathbf{x} - \mathbf{x}'), \quad (5.79)$$

where \mathbf{A}_- is the vector potential corresponding to the difference in magnetic fields \mathbf{B}_- , $\mathbf{B}_- = \nabla \times \mathbf{A}_-$, and we have introduced the phase-breaking rate by hand in view of the above remarks. In the case of the particle-hole ladder, the magnetic-field-induced phases subtract, according to Eq. (5.45), accounting for the appearance of the difference in vector potential, \mathbf{A}_- . For the case of the Cooperon, the particle-particle ladder, the two phases add, and we obtain

$$\left[D \left[-i\nabla - \frac{e}{\hbar} \mathbf{A}_+(\mathbf{x}) \right]^2 + 1/\tau_\phi \right] \tilde{C}_0(\mathbf{x}, \mathbf{x}') = \frac{1}{\tau} \delta(\mathbf{x} - \mathbf{x}'), \quad (5.80)$$

where \mathbf{A}_+ is the vector potential corresponding to the sum of the fields; $\mathbf{B}_+ = \nabla \times \mathbf{A}_+$.

The ‘‘magneto-fingerprint’’ of a given sample, that is, the dependence of its conductance on an external magnetic fields will show an erratic pattern with a given peak-to-valley ratio and correlation field B_c . This, however, is not immediately the information we obtain by calculating the variance,

$$\begin{aligned} \Delta G_{\alpha\beta, \gamma\delta}(\mathbf{B}_+, \mathbf{B}_-) \\ = \langle [G_{\alpha\beta}(\mathbf{B}_1) - \langle G_{\alpha\beta}(\mathbf{B}_1) \rangle][G_{\gamma\delta}(\mathbf{B}_2) - \langle G_{\gamma\delta}(\mathbf{B}_2) \rangle] \rangle, \end{aligned} \quad (5.81)$$

where \mathbf{B}_1 is the field in, say, the inner loop, $\mathbf{B}_1 = \frac{1}{2}(\mathbf{B}_+ + \mathbf{B}_-)$, and \mathbf{B}_2 the field in the outer loop, $\mathbf{B}_2 = \frac{1}{2}(\mathbf{B}_+ - \mathbf{B}_-)$. In the variance (5.81), the magnetic fields are fixed in the two samples, and we are averaging over different impurity configurations, thus describing a situation in which the actual impurity configuration is changed, a hardly controllable endeavor from an experimental point of view. However, if the magnetoconductance of a given sample $G(B)$ varies randomly with magnetic field, the two types of averages—the one with respect to magnetic field and the one with respect to impurity configuration—are equivalent, and the characteristics of the ‘‘magneto-fingerprint’’ can be extracted from the correlation function in Eq. (5.81). The physical

reason for the validity of such an “ergodic” hypothesis (Lee and Stone, 1985), that changing magnetic field is equivalent to changing impurity configuration, is that since the electronic motion in the sample is quantum-mechanically coherent the wave-function pattern is sensitive to the position of all the impurities in the sample, just as the presence of the magnetic field is felt throughout the sample by the electron. The validity of the ergodic hypothesis has been substantiated by Al’tshuler, Kravtsov, and Lerner (1986). The extreme sensitivity to impurity configuration is also witnessed by the fact that changing the position of one impurity by an amount of the order of an atomic distance, $1/k_F$, is equivalent to shifting all the impurities by arbitrary amounts, that is, to create a completely different sample (Al’tshuler and Spivak, 1985; Feng *et al.*, 1986).

To calculate the variance in Eq. (5.81) we must solve Eqs. (5.79) and (5.80) with the mixed boundary value conditions appropriate in the presence of magnetic fields, and insert the solutions into contributions like that in Eq. (5.72). However, determination of the characteristic correlations of the magnetoconductance fluctuations can be done by inspection of Eqs. (5.79) and (5.80). The correlation field B_c is determined by the sample-to-sample change in the magnetic field, that is, \mathbf{B}_- . According to Eqs. (5.79) and (5.80), this field is determined either by the sample size, through the gradient term, or by the phase coherence length. When the phase coherence length is longer than the sample size, the correlation field is therefore of the order of the flux quantum over the sample area, $B_c \sim \phi_0/L^2$, where ϕ_0 is the normal flux quantum $\phi_0 = h/e$, since the typical diffusion loops, like those depicted in Figs. 22 and 23 enclose an area of order the sample size, L^2 . We note that in magnetic fields exceeding $\max\{\phi_0/L^2, \phi_0/L_\phi^2\}$ the Cooperon no longer contributes to the fluctuations, as its dependence on magnetic field is completely suppressed according to the weak-localization analysis.

We end this section by mentioning a few of the interesting physical phenomena discovered in the field of mesoscopic physics. These include, the anomalously large thermoelectric effects in mesoscopic systems due to the breaking of particle-hole symmetry by an impurity configuration (Anisovich *et al.*, 1987); Lesovik and Khmel’nitskii, 1988; Gusev *et al.*, 1990); mesoscopic fluctuations in superconducting-normal-superconducting junctions (Al’tshuler and Spivak, 1987); Aharonov-Bohm oscillations in small rings (Washburn and Webb, 1986); and the possibility of tomography in mesoscopic systems, that is, determining the position of special, for example, bistable, scatterers (Fal’ko and Khmel’nitskii, 1990). The above effects are concerned with the linear-response regime. There are also interesting mesoscopic effects in the nonlinear regime, such as the nonlinear fluctuations in the I - V characteristics of constrictions (Larkin and Khmel’nitskii, 1986), and the photoconductivity effects and the photovoltaic effect in mesoscopic systems (Bykov *et al.*, 1989; Fal’ko, 1989; Fal’ko and Khmel’nitskii,

1989; Bykov *et al.*, 1990).

Just as the phenomenon of weak localization was a general feature of wave propagation in a random medium, the same is equally true of the mesoscopic fluctuation phenomenon. For a recent review of fluctuation effects in the context of classical waves, such as light or sound, we again refer the reader to Shen (1989).

For a complete characterization of the distribution of mesoscopic fluctuations, the presented standard impurity diagram technique is not feasible. Such an analysis, as well as the study of strongly localized systems, the approach to the Anderson transition, requires that one take the impurity average from the outset, and one is led to the study of a field theory, for the present problem the nonlinear sigma model (Al’tshuler, Kravtsov, and Lerner 1991). The result of the analysis, where quantum corrections are included, is to show that certain aspects of mesoscopic fluctuations, such as for example relaxation currents, are nonuniversal and not described by a one-parameter scaling theory.

VI. SUMMARY AND CONCLUSION

We have presented a description of nonequilibrium single-particle states in terms of the density matrix, and shown its relevance to transport phenomena in solids of current interest. The quantum dynamics of a single continuous degree of freedom interacting with various environments was discussed in detail, and the standard Feynman diagrammatic approach developed. The diagrammatic technique made it possible to exhibit the interference aspect of quantum-mechanical motion explicitly. This interference aspect can dominate the transport properties of devices constructable by present day technology, due, for example, to their small size. The general description we have represented was therefore carried out in the spatial representation, which provided a useful pictorial, representation of coherent wave propagation, and allowed proper inclusion of the effects of finite size. The formalism presented should therefore prove useful in future studies of such effects.

The presented diagrammatic technique was used to discuss the intracollisional field effect as an example of the kinetic approach to quantum transport, where such nonlinear effects can be included; both the case of electron-phonon interaction and that of electron-impurity interaction was considered. Within the present formalism the inclusion of the intracollisional field effect was automatic and interpretable in a physically transparent way, as the result of the effect of the external field on the effective interaction of the particle with the environment. The conflicting results in the literature on the intracollisional field effect within the many-body formalisms were identified as the result of the uncontrolled introduction of the quasidistribution function, as such a problem never arose in the present single-particle approach.

In the latter part of the paper we reviewed the theory

of disordered conductors in view of the progress made over the last decade. The simple single-particle approach was shown to be able to account for a vast range of phenomena. The linear-response theory of a noninteracting electron gas was presented using the diagrammatic technique and applied to a discussion of the conductance of macroscopic and mesoscopic samples, with particular emphasis on establishing the physical picture of the quantum interference effects. The weak-localization effect was discussed using the diagrammatic technique developed for the density matrix, thereby in a simple and direct way demonstrating its quantum interference nature. Starting from linear-response theory we showed, by imposing proper boundary conditions, how to arrive at the scattering expression for the conductance of an obstacle, thereby making contact with the Landauer approach to quantum transport. Finally, we discussed the mesoscopic conductance fluctuations, showing their physical origin to be in quantum interference.

The present single-particle approach is of particular relevance for consideration of quantum transport phenomena in bulk semiconductors and structures made of semiconductor material, for which in general we do not have a controllable way of dealing with the complete many-body problem. The simplicity and transparency of the present formalism, however, should make it possible to take advantage of the simplifications pertaining to the particular nonequilibrium situation in question and thereby provide the basis for a consistent treatment of the many-body aspects. The formalism is useful not only in analytical studies, but also for setting up consistent schemes for numerical treatments of transport in complicated realistic material models.

ACKNOWLEDGMENTS

Part of this work was performed while the author benefited from discussions as a member of the quantum transport group of Professor Karl Hess at the University of Illinois. It is a pleasure to thank Professor Anthony J. Leggett for a critical reading of a preliminary version of the manuscript. This research was supported in part by the John D. and Catherine T. MacArthur Foundation at the University of Illinois under Grant No. 0-6-40129 and by the National Science Foundation under Grant No. DMR-86-12860. I thank NORDITA for the hospitality extended to me during the fall of 1989 where part of this work was performed. I thank Dr. Gaute T. Einevoll for inviting me to the University of Trondheim to lecture on results contained in the present article. This research is supported by the Norwegian Research Council for Science and the Humanities. I wish to acknowledge travel support by the NATO Science Fellowships Program, and the reception of a Nordic Research Stipend.

REFERENCES

Abrahams, E., P. W. Anderson, D. C. Licciardello, and T. V. Ramakrishnan, 1979, *Phys. Rev. Lett.* **42**, 673.

- Abrikosov, A.A., L. P. Gor'kov, and I. E. Dzyaloshinski, 1965, *Quantum Field Theoretical Methods in Statistical Physics* (Pergamon, New York).
- Abrikosov, A. A., and I. A. Ryzhkin, 1978, *Adv. Phys.* **27**, 147.
- Afonin, V. V., Yu. M. Galperin, V. L. Gurevich, and A. Schmid, 1987, *Phys. Rev. A* **36**, 5729.
- Al'tshuler, B. L., 1978, *Zh. Eksp. Teor. Fiz.* **75**, 1330 [*Sov. Phys. JETP* **48**, 670 (1978)].
- Al'tshuler, B. L., 1985, *Pis'ma Zh. Eksp. Teor. Fiz.* **41**, 530 [*JETP Lett.* **41**, 648 (1985)].
- Al'tshuler, B. L., and A. G. Aronov, 1981, *Pis'ma Zh. Eksp. Teor. Fiz.* **33**, 515 [*JETP Lett.* **33**, 499 (1981)].
- Al'tshuler, B. L. and A. G. Aronov, 1985, in *Electron-Electron Interactions in Disordered Systems*, edited by A. L. Efros and M. Pollak (North-Holland, Amsterdam), p. 1.
- Al'tshuler, B. L., A. G. Aronov, and D. E. Khmel'nitskii, 1981, *Solid State Commun.* **39**, 619.
- Al'tshuler, B. L., A. G. Aronov, and D. E. Khmel'nitskii, 1982, *J. Phys. C* **15**, 7367.
- Al'tshuler, B. L., A. G. Aronov, D. E. Khmel'nitskii, and A. I. Larkin, 1982, in *Quantum Theory of Solids*, edited by I. M. Lifshitz (MIR, Moscow), p. 130.
- Al'tshuler, B. L., A. G. Aronov, A. I. Larkin, and D. E. Khmel'nitskii, 1981, *Zh. Eksp. Teor. Fiz.* **81**, 768 [*Sov. Phys. JETP* **54**, 411 (1981)].
- Al'tshuler, B. L., A. G. Aronov, and B. Z. Spivak, 1981 *Pis'ma Zh. Eksp. Teor. Fiz.* **33**, 101 [*JETP Lett* **33**, 94 (1981)].
- Al'tshuler, B. L., A. G. Aronov, B. Z. Spivak, D. Yu. Sharvin, and Yu. V. Sharvin, 1982, *Pis'ma Zh. Eksp. Teor. Fiz.* **35**, 476 [*JETP Lett.* **35**, 588 (1982)].
- Al'tshuler, B. L., and D. E. Khmel'nitskii, 1985, *Pis'ma Zh. Eksp. Teor. Fiz.* **42**, 291 [*JETP Lett.* **42**, 359 (1985)].
- Al'tshuler, B. L., D. E. Khmel'nitskii, A. I. Larkin, and P. A. Lee, 1980, *Phys. Rev. B* **22**, 5142.
- Al'tshuler, B. L., V. E. Kravtsov, and I. V. Lerner, 1986, *Pis'ma Zh. Eksp. Teor. Fiz.* **43**, 342 [*JETP Lett.* **43**, 441 (1986)].
- Al'tshuler, B. L., V. E. Kravtsov, and I. V. Lerner, 1991, in *Mesoscopic Phenomena in Solids*, edited by B. L. Al'tshuler, P. A. Lee, and R. A. Webb (Elsevier, Amsterdam), in press.
- Al'tshuler, B. L., and B. I. Shklovskii, 1986, *Zh. Eksp. Teor. Fiz.* **91**, 220 [*Sov. Phys. JETP* **64**, 127 (1986)].
- Al'tshuler, B. L., and B. Z. Spivak, 1985, *Pis'ma Zh. Eksp. Teor. Fiz.* **42**, 363 [*JETP Lett.* **42**, 447 (1985)].
- Al'tshuler, B. L., and B. Z. Spivak, 1986, *Pis'ma Zh. Eksp. Teor. Fiz.* **43**, 185 [*JETP Lett.* **43**, 234 (1986)].
- Al'tshuler, B. L., and B. Z. Spivak, 1987, *Zh. Eksp. Teor. Fiz.* **92**, 609 [*Sov. Phys. JETP* **65**, 343 (1987)].
- Anderson, P. W., 1958, *Phys. Rev.* **102**, 1008.
- Anisovich, A. V., B. L. Al'tshuler, A. G. Aronov, and A. Yu. Zyuzin, 1987, *Pis'ma Zh. Eksp. Teor. Fiz.* **45**, 237 [*JETP Lett.* **45**, 295 (1987)].
- Aronov, A. G. 1984, *Physica B* **126**, 314.
- Aronov, A. G., and Yu. V. Sharvin, 1987, *Rev. Mod. Phys.* **59**, 755.
- Aronov, A. G., A. Yu. Zyuzin, and B. Z. Spivak, 1986, *Pis'ma Zh. Eksp. Teor. Fiz.* **43**, 431 [*JETP Lett.* **43**, 555 (1986)].
- Ashcroft, N. W., and N. D. Mermin, 1976, *Solid State Physics* (Holt, Rinehart and Winston, New York).
- Baranger, H. U., and D. A. Stone, 1989, *Phys. Rev. B* **40**, 8169.
- Baranger, H. U., A. D. Stone, and D. P. DiVincenzo, 1988, *Phys. Rev. B* **37**, 6521.
- Barker, J. R., 1973, *J. Phys. C* **6**, 2663.
- Bending, S. J., K. von Klitzing, and K. Ploog, 1990, *Phys. Rev. Lett.* **65**, 1060.

- Benoit, A., C. P. Umbach, R. B. Laibowitz, and R. A. Webb, 1987, *Phys. Rev. Lett.* **58**, 2357.
- Berezinskii, V. L., 1973, *Zh. Eksp. Teor. Fiz.* **65**, 1251 [*Sov. Phys. JETP* **38**, 620 (1974)].
- Bergmann, G., 1984, *Phys. Rep.* **107**, 1.
- Bertoncini, R., A. M. Krivan, and D. K. Ferry, 1990, *Phys. Rev. B* **41**, 1390.
- Boltzmann, L. W., 1872, *Ber. Wien. Akad.* **66**, 275.
- Boltzmann, L. W., 1896, *Vorlesungen über Gastheorie* (Barth, Leipzig). English translation: *Lectures on Gas Theory* (University of California Press, Berkeley, 1964).
- Brenig, W., M. A. Paalanen, A. F. Hebard, and P. Wölffe, 1986, *Phys. Rev. B* **33**, 1691.
- Bykov, A. A., G. M. Gusev, Z. D. Kvon, D. I. Lubyshev, and V. P. Migal', 1989, *Pis'ma Zh. Eksp. Teor. Fiz.* **49**, 13 [*JETP Lett.* **49**, 13 (1989)].
- Bykov, A. A., G. M. Gusev, and Z. D. Kvon, 1990, *Zh. Eksp. Teor. Fiz.* **97**, 1317 [*Sov. Phys. JETP*, **70**, 742 (1990)].
- Büttiker, M., 1986a, *Phys. Rev. Lett.* **57**, 1761.
- Büttiker, M., 1986b, *Phys. Rev. B* **33**, 3020.
- Büttiker, M., 1988, *Phys. Rev. B* **38**, 9375.
- Caldeira, A. O., and A. J. Leggett, 1983, *Ann. Phys. (N.Y.)* **149**, 374.
- Callen, H. B., and T. A. Welton, 1951, *Phys. Rev.* **83**, 34.
- Chakravarty, S., and A. Schmid, 1986, *Phys. Rep.* **140**, 193.
- Datta, S., 1989, *Superlatt. Microstruct.* **6**, 86.
- Dugaev, V. K., and D. E. Khmel'nitskii, 1984, *Zh. Eksp. Teor. Fiz.* **86**, 1784 [*Sov. Phys. JETP* **59**, 1038 (1984)].
- Eckern, U., and A. Schmid, 1981, *J. Low Temp. Phys.* **45**, 137.
- Edwards, S.F., 1958, *Philos. Mag.* **3**, 1020.
- Efetov, K., 1983, *Adv. Phys.* **32**, 53.
- Eiler, W., 1984, *J. Low Temp. Phys.* **56**, 481.
- Eiler, W., 1985, *Solid State Commun.* **56**, 917.
- Eliashberg, G. M., 1971, *Zh. Eksp. Teor. Fiz.* **61**, 1254 [*Sov. Phys. JETP* **34**, 668 (1972)].
- Engquist, H. L., and P. W. Anderson, 1981, *Phys. Rev. B* **24**, 1151.
- Fal'ko, V. I., 1987, *Zh. Eksp. Teor. Fiz.* **92**, 704 [*Sov. Phys. JETP* **65**, 397 (1987)].
- Fal'ko, V. I., 1989, *Europhys. Lett.* **8**, 785.
- Fal'ko, V. I., and D. E. Khmel'nitskii, 1989, *Zh. Eksp. Teor. Fiz.* **95**, 328 [*Sov. Phys. JETP* **68**, 186 (1989)].
- Fal'ko, V. I., and D. E. Khmel'nitskii, 1990, *Pis'ma, Zh. Eksp. Teor. Fiz.* **51**, 166 [*JETP Lett.* **51**, 189 (1990)].
- Feng, S., 1990, *Phys. Lett. A* **143**, 400.
- Feng, S., P. A. Lee, and D. A. Stone, 1986, *Phys. Rev. Lett.* **56**, 1960; **56**, 2772(E).
- Feynman, R. P., R. W. Hellwarth, C. K. Iddings, and P. M. Platzman, 1962, *Phys. Rev.* **127**, 1004.
- Feynman, R. P., and A. R. Hibbs, 1965, *Quantum Mechanics and Path Integrals* (McGraw-Hill, New York).
- Feynman, R. P., and F. L. Vernon, Jr., 1963, *Ann. Phys. (N.Y.)*, **24**, 118.
- Fisher, D. S., and P. A. Lee, 1981, *Phys. Rev. B* **23**, 6851.
- Geim, A. K., 1989, *Pis'ma Zh. Eksp. Teor. Fiz.* **50**, 359 [*JETP Lett.* **50**, 389 (1989)].
- Glazman, L. I., G. B. Lesovik, D. E. Khmel'nitskii, and R. I. Shekter, 1988, *Pis'ma Zh. Eksp. Teor. Fiz.* **48**, 218 [*JETP Lett.* **48**, 238 (1988)].
- Gordon, J. M., 1984, *Phys. Rev. B* **30**, 6770.
- Gor'kov, L. P., A. I. Larkin, and D. E. Khmel'nitskii, 1979, *Pis'ma, Zh. Eksp. Teor. Fiz.* **30**, 248 [*JETP Lett.* **30**, 228 (1979)].
- Gradshteyn, I. S., and I. M. Ryzhik, 1980, *Table of Integrals, Series, and Products* (Academic, New York).
- Greenwood, D. A., 1958, *Proc. Phys. Soc. London, Ser. A* **71**, 585.
- Gusev, G. M., Z. D. Kvon, and A. G. Pogosov, 1990, *Pis'ma Zh. Eksp. Teor. Fiz.* **51**, 151 [*JETP Lett.* **51**, 171 (1990)].
- Hershfield, S., 1989, *Ann. Phys. (N.Y.)* **196**, 12.
- Hershfield, S., and V. Ambegaokar, 1988, *Phys. Rev. B* **38**, 7909.
- Hikami, S., A. I. Larkin, and Y. Nagaoka, 1980, *Prog. Theor. Phys.* **63**, 707.
- Iche, G., and P. Nozières, 1978, *Physica A* **91**, 485.
- Imry, Y., 1986, in *Directions in Condensed Matter Physics* Vol. 1, edited by G. Grinstein and G. Mazenko (World Scientific, Singapore), p. 101.
- Jauho, A.-P., 1991, in *Granular Nanoelectronics*, NATO Advanced Study Institute Series B, Vol. 91, edited by D. K. Ferry, J. R. Barker, and C. Jacoboni (Plenum, New York/London), p. 133.
- Jauho, A.-P., and J. W. Wilkins, 1984, *Phys. Rev. B* **29**, 1919.
- Kadanoff, L. P., and G. Baym, 1962, *Quantum Statistical Mechanics* (Benjamin, New York).
- Kadanoff, L. P., and M. Revsen, 1964, *Nuovo Cimento* **33**, 397.
- Kane, C. L., P. A. Lee, and D. P. DiVincenzo, 1988, *Phys. Rev. B* **38**, 2995.
- Kane, C. L., R. A. Serota, and P. A. Lee, 1988, *Phys. Rev. B* **37**, 6701.
- Kawabata, A., 1980, *J. Phys. Soc. Jpn.* **49**, 628.
- Kawabata, A., 1984, *J. Phys. Soc. Jpn.* **53**, 3540.
- Keldysh, L. V., 1964, *Zh. Eksp. Teor. Fiz.* **57**, 660 [*Sov. Phys. JETP* **20**, 1018 (1965)].
- Khmelnitskii, D. E., 1984, *Physica B* **126**, 235.
- Kohn, W., and J. M. Luttinger, 1957, *Phys. Rev.* **108**, 590.
- Konstantinov, O. V., and V. I. Perel, 1960, *Zh. Eksp. Teor. Fiz.* **39**, 197 [*Sov. Phys. JETP* **12**, 142 (1961)].
- Kubo, R., M. Toda, and N. Hashitsume, 1983, *Statistical Physics II. Nonequilibrium Statistical Mechanics* (Springer, Berlin).
- Landau, L.D., 1927, *Phys. Z. Sowjetunion* **45**, 430.
- Landau, L. D., and I. M. Lifshitz, 1965, *Quantum Mechanics* (Pergamon, New York).
- Landau, L. D., and I. M. Lifshitz, 1980, *Statistical Physics* (Pergamon, New York).
- Landauer, R., 1957, *IBM J. Res. Dev.* **1**, 233.
- Landauer, R., 1970, *Philos. Mag.* **21**, 863.
- Landauer, R., 1985, in *Localization, Interaction, and Transport Phenomena*, Springer Series in Solid-State Sciences No. 61, edited by B. Kramer, G. Bergmann, and Y. Bruynseraede (Springer, New York), p. 38.
- Langer, J. S., 1960, *Phys. Rev.* **127**, 1004.
- Langer, J. S., and T. Neal, 1966, *Phys. Rev. Lett.* **16**, 984.
- Langreth, D. C., 1967, *Phys. Rev.* **159**, 717.
- Langreth, D. C., and E. Abrahams, 1981, *Phys. Rev. B* **24**, 2978.
- Larkin, A. I., 1980, *Pis'ma Zh. Eksp. Teor. Fiz.* **31**, 239 [*JETP Lett.* **31**, 219 (1980)].
- Larkin, A. I., and D. E. Khmel'nitskii, 1982, *Usp. Fiz. Nauk* **136**, 536 [*Sov. Phys. Usp.* **25**, 185 (1982)].
- Larkin, A.I., and D. E. Khmel'nitskii, 1986, *Zh. Eksp. Teor. Fiz.* **91**, 1815 [*Sov. Phys. JETP* **64**, 1075 (1986)].
- Lax, M., 1958, *Phys. Rev.* **109**, 1921.
- Lee, P. A., and T. V. Ramakrishnan, 1985, *Rev. Mod. Phys.* **57**, 287.
- Lee, P. A., and A. D. Stone, 1985, *Phys. Rev. Lett.* **55**, 1622.
- Lee, P. A., A. D. Stone, and H. Fukuyama, 1987, *Phys. Rev. B* **35**, 1039.
- Lesovik, G.B., and D. E. Khmel'nitskii, 1988, *Zh. Eksp. Teor.*

- Fiz. **94**, 164 [Sov. Phys. JETP **67**, 957 (1988)].
- Levinson, I. B., 1969, Zh. Eksp. Teor. Fiz. **57**, 660 [Sov. Phys. JETP **30**, 362 (1970)].
- Lipavsky, P., V. Spicka, and B. Velicky, 1986, Phys. Rev. B **34**, 6933.
- Martin, P. C., and J. Schwinger, 1959, Phys. Rev. **115**, 1342.
- Mason, B. A., and K. Hess, 1989, Phys. Rev. B **39**, 5051.
- Mills, R., 1969, *Propagators for Many-Particle Systems* (Gordon and Breach, New York).
- Prange, R. E., and L. P. Kadanoff, 1964, Phys. Rev. **134**, 566A.
- Rainer, D., and G. Bergmann, 1985, Phys. Rev. B **32**, 3522.
- Rammer, J., and A. Schmid, 1986, Phys. Rev. B **34**, 1352.
- Rammer, J., and A. L. Shelankov, 1987, Phys. Rev. B **36**, 3135.
- Rammer, J., 1985, Ph.D. thesis (University of Copenhagen).
- Rammer, J., and H. Smith, 1986, Rev. Mod. Phys. **58**, 323.
- Ravenhall, D. G., H. W. Wyld, and R. L. Schult, 1989, Phys. Rev. Lett. **62**, 1780.
- Schmid, A., 1985, in *Localization, Interaction and Transport Phenomena*, Springer Series in Solid-State Sciences No. 61 edited by B. Kramer, G. Bergmann, and Y. Bruynseraede, (Springer, New York), p. 212.
- Schwinger, J., 1961, J. Math. Phys. (N.Y.) **2**, 407.
- Serene, J. W., and D. Rainer, 1983, Phys. Rep. **101**, 221.
- Serota, R. A., 1988, Phys. Rev. B **38**, 12640.
- Serota, R.A., S. Feng, C. Kane, and P. A. Lee, 1987, Phys. Rev. B **36**, 5031.
- Shelankov, A. L., 1985, J. Low. Temp. Phys. **60**, 29.
- Shen, P., 1989, Ed., *Scattering and Localization of Classical Waves in Random Media* (World Scientific, Singapore).
- Skocpol, W. J., P. M. Mankiewich, R. E. Howard, L. D. Jackel, D. M. Tennant, and D. A. Stone, 1987, Phys. Rev. Lett. **58**, 2347.
- Sols, F., M. Macucci, U. Ravaioli, and K. Hess, 1989, J. Appl. Phys. **66**, 3892.
- Spivak, B. Z., and D. E. Khmel'nitskii, 1982, Pis'ma Zh. Eksp. Teor. Fiz. **35**, 334 [JETP Lett. **35**, 412 (1982)].
- Stone, A. D., 1985, Phys. Rev. Lett. **55**, 2692.
- Szafer, A., and A. D. Stone, 1989, Phys. Rev. Lett. **62**, 300.
- Thornber, K. K., and R. P. Feynman, 1970, Phys. Rev. B **1**, 4099.
- Thouless, D. J., 1981, Phys. Rev. Lett. **47**, 972.
- Umbach, C. P., S. Washburn, R. B. Laibowitz, and R. A. Webb, 1984, Phys. Rev. B **30**, 4048.
- van Wees, B. J., H. van Houten, C. W. Beenakker, J. G. Williamson, L. P. Kouwenhoven, D. van der Marel, and C. T. Foxen, 1988, Phys. Rev. Lett. **60**, 848.
- Vitkalov, S. A., G. M. Gusev, Z. D. Kvon, G. I. Leviev, and V. I. Fal'ko, 1988, Zh. Eksp. Teor. Fiz. **94**, 376 [Sov. Phys. JETP **67**, 1080 (1988)].
- von Neumann, J., 1932, *Mathematische Grundlagen der Quantenmechanik* (Springer, Berlin). English translation: *Mathematical Foundations of Quantum Mechanics* (Princeton University, Princeton, NJ, 1955).
- Wang, S., and P. E. Lindelof, 1987, Phys. Rev. Lett. **59**, 1156.
- Washburn, S., and R. A. Webb, 1986, Adv. Phys. **35**, 375.
- Watson, K. M., 1969, J. Math. Phys. **10**, 688.
- Webb, R. A., S. Washburn, C. P. Umbach, and R. B. Laibowitz, 1985a, in *Localization, Interaction, and Transport Phenomena*, Springer Series in Solid-State Sciences No. 61, edited by B. Kramer, G. Bergmann, and Y. Bruynseraede (Springer, New York), p. 121.
- Webb, R. A., S. Washburn, C. P. Umbach, and R. B. Laibowitz, 1985b, Phys. Rev. Lett. **55**, 2696.
- Wegner, F., 1979, Z. Phys. B **35**, 207.
- Wheeler, J. A., and W. H. Zurek, 1983, Eds., *Quantum Theory and Measurement* (Princeton University, Princeton, NJ).
- Wigner, E., 1932, Phys. Rev. **40**, 749.
- Wittmann, H.-P., and A. Schmid, 1987, J. Low. Temp. Phys. **69**, 131.